Charges on Polymeric Insulators and Their Effect on Flashover Characteristics

by

MEBRAHTU MELAKE SEMERE

Diploma work No. 47/2011
Department of Materials and Manufacturing Technology
CHALMERS UNIVERSITY OF TECHNOLOGY
Gothenburg, Sweden

Master Thesis in ELECTRIC POWER ENGINEERING

Performed at: **Chalmers University of Technology**
SE-41296 Göteborg, Sweden

Supervisor/Examiner: Associate Professor Yuriy Serdyuk
Department of Materials and Manufacturing Technology
Division of High Voltage Engineering
Chalmers University of Technology
SE-412 96 Gothenburg, Sweden

Charges On Polymeric Insulators And Their Effect On Flashover Characteristics
MEBRAHTU MELAKE SEMERE

Diploma work no 47/2011
Department of Materials and Manufacturing Technology
Division of High Voltage Engineering
Chalmers University of Technology
SE-412 96 Gothenburg, Sweden
Telephone + 46 (0)31-772 1000

Chalmers Reproservice
Gothenburg, Sweden 2011

Charges on Polymeric Insulators and Their Effect on Flashover Characteristics
MEBRAHTU MELAKE
Department of Materials and Manufacturing Technology
Chalmers University of Technology

ABSTRACT

Nowadays polymeric materials are widely applied in outdoor high voltage insulation systems gradually replacing traditionally used porcelain and glass. It is believed that polymer based insulation will become dominant at ultra high voltages, e.g. in 1000 kV ac and 800 kV dc overhead transmission lines, which are presently being developed. Although withstand performance of polymeric insulating materials has been studied over the years, there is still a lack of complete physical understanding of all important aspects related to practical situations. Thus, the behavior and performance of polymeric materials for high-voltage applications in presence of accumulated surface charges, which can be generated in practice due to different sources (e.g. corona, surface discharges, space charge build-up, etc), are not completely understood today. This phenomenon needs to be considered when designing insulation systems and when performing insulator testing, especially for high-voltage dc (HVDC) applications where presence of surface charges is the inherent property of the system.

The research conducted within the thesis project focused on experimental investigations of the influence of pre-deposited surface charges on impulse flashover characteristics of polymeric model insulators in air. The study also involved development of surface charge deposition system based on dc corona discharge as well as measurements of charge dynamics and its relaxation on cylindrical polymeric insulators made of poly-dienethylsiloxane based rubber, so called Silicon Rubber (SIR) and Room Temperature Vulcanized Silicon Rubber (RTV-SIR) based rubber, which are widely used in outdoor high voltage insulation systems.

The results presented and discussed in the report indicate that the presence of charges on surfaces of polymeric insulators can lead to a decrease or an increase of insulator withstand voltages depending on the polarities of the deposited surface charges and applied impulse voltages.

Keywords: Surface charge, material properties, surface potential measurement, impulse flashover voltage, dc corona charging, charge relaxation, surface potential decay.

ACKNOWLEDGMENTS

This thesis has been carried out at Division of High Voltage Engineering under Department of Materials and Manufacturing Technology of Chalmers University of Technology.

First and for most I would like to extend my profound gratitude to my examiner/supervisor Ass. Prof. Yuriy Serdyuk, for his valuable guidance, inspiration and assistance throughout this thesis work. He had motivated me to do more by bringing new ideas and finally shaping my report, and was always there when I need him. Without his encouragement and constant guidance I could not have complete this thesis. I also express my indebted gratitude to Prof. Stanislaw Gubanski, the Head of Division of High Voltage Engineering.

My special thanks to Sarath Kumara, who guided me during the measurement period and provided me with all the information that was needed for treatment of the measurement results. He also put a great effort to analyze the measurement results with the simulation using Comsol software. I also like to pass my thanks to Shahid Alam, who assisted me during part of the laboratory measurements.

I would like to thank all my friends and colleagues at the Department at Chalmers, in thesis room for making my thesis work period more comfortable, pleasant and also for creating friendly atmosphere to discuss problems related to the thesis.

Finally, yet importantly, I would like to express my deepest appreciation to my parents and my wife who gave me endless support and inspiration to continue with this study at abroad.

Mebrahtu Melake Semere

TABLE OF CONTENTS

ABBREVIATIONS

DC	Direct Current
DPR	Detail Project Report
PDMS	Polydimethylsiloxane
EPDM	Ethyl-propylene-dine –monomer
EHV	Extra High Voltage
FOV	Flashover Voltage
GIS	Gas Insulated System
HV	High voltage
HVDC	High Voltage direct current
HDPE	High density polyethylene
KV	Kilo Volt
KVA	Kilo Volt Ampere
LI	Lightning Impulse
NLI	Negative Lightning Impulse
PLI	Positive Lightning Impulse
RTV-SIR	Room temperature vulcanized silicon rubber
SIR	Silicon Rubber
VT	Voltage Transformer
WSDV	Withstand voltage
$U_{50\,\%}$	50% flashover voltage

CHAPTER 1

1. INTRODUCTION

1.1.Background and Motivation

In the modern society the development of the ultra high voltage transmission system is an important step to supply consumers with electric power. The high voltage direct current (HVDC) technology is seen today as the most suitable solution when longer distances are involved [1]. It has been explained in the Energy Market 2010 that, the Energy Consumption worldwide will increase by about 49% within the next 25 years [2]. As a consequence of this, the voltage levels are prone to be increased to meet these energy demands and therefore, the insulation system will be subjected to higher electrical stresses than ever before. Hence, new materials which have a better insulation performance, lower weight and reduced loss should have to be used. Polymeric materials such as polydiemethylsiloxane based rubber, popularly called silicon Rubber (SIR) and ethyl-propylene-diene-monomer (EPDM) based rubber are widely applied in outdoor high voltage insulation systems. These materials are gradually replacing traditionally used porcelain and glass insulators. It is believed that polymer based insulation will become dominant at ultra high voltages, e.g. in 1000 kV ac and 800 kV dc overhead transmission lines, which are presently being developed. Although withstand performance of polymeric insulating materials has been studied over the years, there is still a lack of complete physical understanding of all important aspects related to practical situations. Thus, one of the obstacles in using polymeric materials for high-voltage applications is a lack of knowledge on their behavior and properties in presence of accumulated surface charges, which can be generated in practice due to different sources (e.g. corona, surface discharges, space charge build-up, etc) activated under extremely high field conditions. This phenomenon needs to be considered when designing insulation systems and when performing insulator testing, especially for high-voltage dc (HVDC) applications where presence of surface charges is the inherent property of the system.

1.2. Objective of the thesis

The aim of the thesis project is to investigate the influence of pre-deposited surface charges on flashover characteristics of polymeric insulators in air. It is expected to strengthen our knowledge and understanding of behavior of polymeric insulators in presence of charges on their surfaces required for development of HVDC insulation systems.

1.3. Procedure and Outcome

The study involves characterization of materials used for model insulators, developing surface charge deposition and measuring system, and measuring flashover characteristics of model insulators under impulse and external dc corona charging conditions.

1.4. Outline of the Thesis

This master's thesis work was divided in to five main chapters.

Chapter 1, Presents an overall introduction of the subject, the background and motivation for carrying out thesis and its objectives. It also describes the scope of the work.

Chapter 2, Presents a general literature analysis on charging mechanisms Here charge accumulation on the surfaces of polymeric materials, charges dynamics and decay mechanisms, flashover performance of insulating polymers in the presence of deposited surface charges are discussed.

Chapter 3, Presents experimental work done on the deposition of surface charges and decay processes for samples stressed by LI voltage and dc corona charged surfaces of RTV-SIR and SIR polymer materials under normal temperature and pressure in atmospheric air.

Chapter 4, Discuses and compares the experimental results performed for the FOV test in the presence of deposited surface charges under the impulse voltage application and on a dc corona charged surfaces of RTV-SIR and SIR polymer materials under normal temperature and pressure in atmospheric air.

Chapter 5, Conclusion and recommendations on the findings are made and suggestions for future studies on the work are proposed.

CHAPTER 2

2. OVERVIEW OF CHARGING AND DECAY MECHANISMS ON POLYMERIC MATERIALS

2.1.Charging mechanisms of polymeric insulators

Surface charge accumulation and decay on dielectric surfaces represent a topic which has been studied extensively, but still needs more detail investigations in some aspects. It is commonly accepted today that there is no single dominating process behind charge accumulation on polymeric surfaces; instead, several of them are responsible for the phenomenon [5-10]. In general, charging of insulating materials may occur due to external reasons, such as corona discharges, surface discharges from metallic particles in a contaminated medium, partial discharges near contaminating particles, defects near the triple junction, and also due to internal space charge build-up due to inhomogeneity of an insulating material in the presence of electric field, charges appearing at the interface between two materials having different permitivities and conductivities, etc. Generation and decay of surface charges depends on the nature and state of the gas medium (temperature, pressure and humidity), the morphology of the electrode set-up, the magnitude and duration of the applied potential, etc. Among these sources, corona discharges are the most common in practice and they often used for research purposes providing effective generation of high amount of free charge carriers in an initially electrically neutral gas volume [3,4,14,18]. As it is known, coronas occur when the electric field strength at the surface of the corona electrode exceeds the ionization threshold of the gas and it is associated with a number of elementary processes in air like natural ionization (due to radioactivity of Earth, irradiation, etc.), impact ionization of neutral atoms/molecules by electrons, photoionization, attachment of electrons to neutral molecules, detachment of electrons from negative ions, recombination between opposite charges, emissions from the electrodes and secondary feedbacks from the cathode [4, 11]. A description of the mechanisms mentioned above is presented below.

Background ionization

Theoretically, at normal temperature and pressure, gases are excellent insulators (no conduction current). But this is not observed in practice. Gases consist of mostly neutral molecules and small amount of charged particles, heavy ions (either positive or negative) and free electrons, all moving randomly and if we apply even a few volts to a uniform field air gap, we can detect a very small conduction current, which is in the order of $10^{-10}\mathrm{A}/m^2$. The source of this ionization current might be due to cosmic radiation and radioactive substances present in the atmosphere and the earth. The generated charges stay in equilibrium under low field condition. The rate of background ionization (S_0) is 10^6-10^7 ion pairs/ ($m^3.s$) that leads to permanent presence of about 10^9 ion pairs/m^3 [4, 13-16].

Electron impact ionization

Electron impact ionization is the most important charge generation mechanism in the bulk of a gas discharge [12]. Its rate of growth can be characterized by Townsends ionization coefficient α, that is

the number of ionization events occurred by a single electron per unit length path along the field. That is, if the applied electric field is high enough to accelerate the electrons, at a certain field strength non-elastic collision takes place between these electrons and natural atoms/or molecules. Ones the electron energy gained from the field during the movement between collisions, is high enough to ionize the gas molecule or atom (i.e. the gained electron energy is greater than ionizing energy $(\Delta W \geq eV_i)$); new electrons and positive ions will be generated according to the reaction $A+e \rightarrow A^{+}+2e$. Here *A,* A^{+} *and e* stands for the neutral particle, positive ion and electron, respectively. The rate of generation of positive ions and electrons can be denoted as; $dn/dt = \alpha\, n_e n_p$. Here $n_e$and $n_p$represent concentration of electrons and positive ions respectively. The ionization coefficient α is a field dependent quantity and its value for different gases can be found from the literatures and measured data [4, 13,-16].

Attachment

This process is sometimes the main mechanism for electronic losses in electronegative gases and in gas mixtures containing electronegative additives. It depends on the energy of the electron and the nature of the gas and is a very important process from the engineering point of view. The procedures under gone to the mechanism can be explained as follows; since certain atoms or molecules in their gaseous state can readily acquire free electron to form a stable negative ion. This type of collisions in which electrons may become attached to atoms or molecules to form negative ions are called attachment collisions, which results in removing of electrons from the gas and generation of the negative ions according to the reaction AB +e <=>A^{-} + B. Here AB, B and A^{-}stands for the neutral molecule, neutral atom, and negative ion, respectively.
The rate of attachment can be characterized using attachment coefficient*, η,* which is similar to α for ionization process. *η* is strongly field dependent and corresponding quantities for the different gases can be found in the literature [4, 13,-16].

Detachment

This process is opposite to the attachment process. Collisions of negative ions with active particles may result in a release of electrons, which is an additional to (impact ionization) mechanism of generation of electrons. Detachment can be characterized by detachment rate coefficient, K_{det}, or detachment frequency, v_{det}, ($v_{det} = K_{det}N$)which can be found as a function of temperature or reduced electric field (E/P or E/N). Where *E, P* and *N* represent electric field, pressure and gas density respectively [3,16]. The rate of generation of electrons (loss of negative ions) can further be obtained as $dn/dt = v_{det}\, n_n$.

Recombination

As the concentration of both ions and electros are significant in the bulk of a gas discharge, there is a probability for electrons to recombine with positive ions upon collisions. This process may take place at a certain energy of electrons and, depending on the way in which the excess energy is released, different types of electron-ion recombination reactions can be identified:

(1) $A^{+} + e \rightarrow A + hv$ *or* $A^{+} + e \rightarrow A^{m} + hv - radiative\ recombination$
(2) $A^{+}B + e \rightarrow A^{m} + B - dissiciative\ recombination$
(3) $A^{+} + e + e \rightarrow A + e - three\ body\ recombination$

Here, $A^m$and hv represent excited state of an atom and released quantum energy, respectively. Dissociative recombination is the fastest bulk recombination mechanism in weakly ionized plasma, such as glow discharge [16, 20]. Electron-ion recombination results in loss of both electrons and positive ions with a rate of $dn/dt = \beta_{ei} n_e n_p$.The recombination coefficient, β_{ei}, is about $5.\ 10^{-8}\ cm^3 s^{-1}$ for air under normal conditions.

Recombination between negative and positive ions normally takes place in electronegative gases, where negative ions are present. At low pressure, ion-ion recombination happens through two body collisions, whereas at moderate pressures it occurs through three body collisions. The rate of loss of positive and negative ions can be calculated as $dn/dt = \beta_{ii} n_n n_p$. The ion-ion recombination coefficient, β_{ii} for air at atmospheric pressure is defined in the literature as a function of ion temperature [4, 17].

Charge transport processes

Mechanisms which are considered in the transport of free charges are drift and diffusion. Both of them can contribute to accumulation of charge carriers on polymeric insulator surfaces.

Drift

Application of an external field to a gas containing charged particles results in their movement in the direction (or opposite, depending on the sign of the charge) of the applied field in addition to their random motion. This movement is called drift and its average velocity, called drift velocity **w**, depends on the applied field, the charge and the mass of the particles involved, pressure etc. The ratio of the drift velocity to the electric field strength is known as mobility, $\boldsymbol{\mu}$, and it is widely used to characterize the charge transport due to drift. Typically the mobility is field dependent for most of the gases [4, 13].

Diffusion

In electrical discharges, whenever there is a non uniform concentration of ions there will be movement of ions from region of higher concentration to regions of lower concentration in order to minimize the concentration gradient. The process by which equilibrium is achieved is called diffusion, which is characterized by the corresponding rate coefficient D [18]. In the case of electron transport in gas discharge plasma, the value of D can be estimated by the well known Einstein relation $\boldsymbol{\mu} = KT/\boldsymbol{q}$, which is valid up to very strong field strength values. Here k, T and q stand for Boltzmann's constant, temperature of gas plasma and elementary charge respectively.

Charges deposited on the surface of polymeric insulators

The accumulation of free charges on an insulating surface is dependent on the intensity of the sources of free charges, how effectively they are transported to the surface and on the rate of their decay [12, 19]. The net collected density of charges is then defined by the difference between the rate of arrival and the rate of decay of charges. During charging, the rate of charge deposition is faster than the decay rate that may be due to the high resistivity value of the dielectric materials used as insulators. The loss of charges, which may appear e.g. due to surface conduction or other decay processes, usually lasts hours rather than seconds, which is the expected time scale for charge accumulation on dielectric surfaces. The deposited charges induce surface potential $V_s(t)$, whose magnitude (in case of a polymer film of thickness d and permittivity ε) at time t after the onset of charging is given by the equation 2.1 [20].

$$\boldsymbol{V_s(t)}\ \frac{\mathbf{dQ}}{\varepsilon}+\frac{1}{\varepsilon}\int_0^d(d-x)\rho(x,t)dx \qquad (2.1)$$

Here, Q (t) is the charge density in surface states and ρ(x, t) is the density of injected bulk charge at a distance *x* below the surface. For simplicity, only variation of field strength (charges magnitude) normal to the surface has been considered.

The relationship between Q (t) and ρ(x, t) is complicated and it is affected by the rates of deposition and injection of charges, the field and the mobility of charges in the bulk. At the end of the charging period t_c and depending on these conditions, Q (t_c) and $\int_0^d(d-x)\rho(x,t)dx$ will have values which control the subsequent discharge processes and the decay of V_s (t_c). It is to be expected that the bulk charge will decay more rapidly than the surface charge and thus the decay of $V_s(t_c)$ will follow some composite law reflecting the relative magnitudes of Q(t_c) and $\int_0^d(d-x)\rho\ (x,t)dx$.

Charges deposited due to interfacial polarization

The gas-solid system can be considered as a material with inhomogeneous permittivity and conductivity. For such a combination, a charge accumulated on interfaces can be deduced from Maxwell and Ohm laws

$\boldsymbol{\nabla}\times\mathbf{E}=0$ (a)

$\nabla.\ \varepsilon_0\varepsilon_r E=\boldsymbol{\rho}$ (b)

$\nabla.\ \mathbf{J}+\frac{\partial\boldsymbol{\rho}}{\partial\mathbf{t}}=0$ (c) (2.2)

$J=\boldsymbol{\sigma}\ \mathbf{E}$ (d)

Here, ε_0 represents the permittivity in free space, ε_r is the relative permittivity of the material, **E** is the applied electric field, $\boldsymbol{\rho}$ is the space charge density, **J** is the current density and $\boldsymbol{\sigma}$ is the conductivity. By combining equation (2.2) b, c and d, the charge density can be described as

$$\boldsymbol{\rho}=\varepsilon_0\ \varepsilon_r\mathbf{E}\ .\ [\ \frac{\nabla\varepsilon_r}{\varepsilon_r}-\frac{\nabla\sigma}{\sigma}\ ] \qquad (2.3)$$

Hence, for materials with varying ε_r and $\boldsymbol{\sigma}$, charges may accumulate on interfaces if the overlapped materials are stressed by an electric field. This can be illustrated in Figure 2.1. The charge density and its dynamic behavior in the system considered can be represented by the following equation derived in (2.4) b and c

$\varepsilon_1 E_{n1}-\varepsilon_2 E_{n2}=\delta$ (a)

$\sigma_1 E_{n1}-\sigma_2 E_{n1}=-\frac{\partial\delta}{\partial t}$ (b) (2.4)

$\frac{\partial\delta}{\partial t}+\frac{\delta}{\frac{\varepsilon_2}{\sigma_2}}=\frac{\varepsilon_1}{\frac{\varepsilon_2}{\sigma_2}}E_{n1}-\sigma_1 E_{n1}$ (c)

Here δ, is the surface charge density, the subscript n, denotes the normal component of the field to the interface and the subscripts 1and 2 denote respectively the different dielectric materials on both sides of the interface.

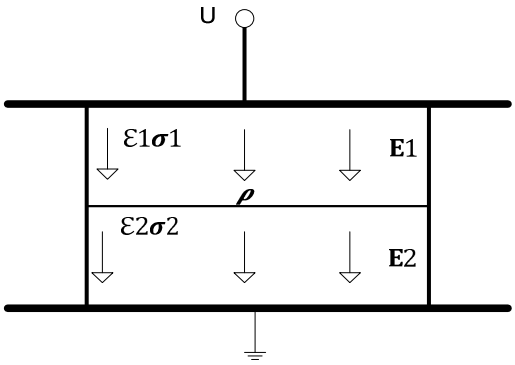

Figure 2.1.Schematic view of charge accumulation at an interface of two materials E_1 and E_2 are the electric field strength, ε_1 and ε_2 are the permittivity respectively for the different materials and ρ is the surface charge density

Some similarity can be observed when a solid–gas interface is exposed to a corona discharge, as illustrated in the Figure 2.2. Despite the non-uniform field distribution, the charge transport through the gas phase is strongly field dependent. Hence the charges are accumulated on the surface of the solid material with specific density and spread on the surface depending on the electric field level, geometry of the electrodes, time of applied voltage, etc.

Many investigations have been conducted within the area of surface charging and charge formation under an extensive period of time and some important experimental results and suggested models of the physical processes involved are reviewed in [3, 4-10]. Although the reviewed papers address the difficulties of explaining the different charging mechanisms based on their simulation models and experimental results, they still have some correlations. Generally, it is hard to consider all the parameters simultaneously hence most of the referred investigations had limitations in providing a detail understanding of the mechanisms. This might be due to the fact that the source of the charges and the interfacing media used were not the same (like SF6-dielectric interface, compressed air-dielectric, and few of them use atmospheric air/ dielectric interfaces, etc).

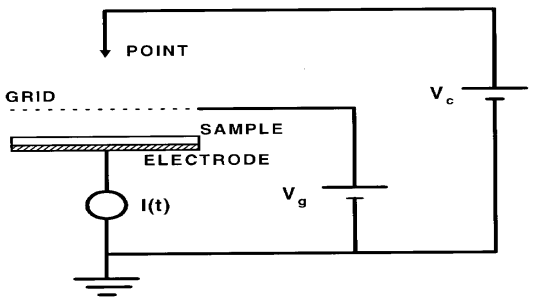

Figure 2.2. Schematic diagram of a simple corona triode. A metallic point is connected to a HV supply. A grid, biased by a voltage supply, is inserted into the gap between the metallic point and the sample surface. I(t) is the measured charging current that can be controlled

In addition to that, the electrode-arrangements used for the experiments/simulations were mostly of traditional types (i.e., a point-plane, and rod (wire)-plane arrangements). Its well known that the geometrical arrangement of the set-up has a strong effect on the distribution of the electric field. Therefore, plane electrode system is normally used for studies of polarization while a needle-plane or point-plane configuration is often utilized for corona charging. The electrode set up utilized in many experimental investigations on corona charging is illustrated in the Figure 2.2. The general idea of this method is to provide a uniform charge distribution on the surface of the dielectric material and to control the potential of the charged surfaces. The sample potential (usually measured along the dielectric surface) can also be deduced from the grid voltage [18]. Although this geometrical arrangement has been practiced for a long period of time, it seems more ideal as compared to the real outdoor insulators which have been utilized at present. Similarly, it is clearly defined by many authors that an electrode arrangement has a great effect in modifying the electric field, which may also have an effect on the charging and discharge process along the surface of the insulators (the charging and decay mechanisms will be somehow affected as well). The set up used in present experimental work is made to represent the real insulators and a more detailed analysis will be given in the next chapter.

2.2. Surface charge relaxation on polymeric materials

Since the discovery of the so-called cross-over phenomena by [27] in his decay measurement on thin untreated polyethylene films in 1967, surface potential decay have attracted the interest of many physicists and engineers in the last decades. This interest has increased radically, especially with the application of polymeric insulators as an outdoor insulator and due to their continuous operation at ultra high voltages. Hence, a deeper understanding of the decay processes on dielectric materials and the parameters responsible for the mechanism provides a convenient way for the determination of the electrical properties of insulating materials. This will enhance their applications especially in HVDC and ultra HV areas, which are radically growing at the present due to the significant increase of energy consumption worldwide and far distances between the generation and distribution locations. Although the mechanisms responsible for the surface charge decay have been studied by many authors [25, 26], the available knowledge is not consistent yet. This may be due to the lack of understanding on a common effect of a large number of simultaneously exiting physical processes taking place on dielectric surfaces during charge decay.

In general, there are three possibly responsible for the surface decay mechanism on corona-charged polymeric insulators: charge neutralization by gas ions, electric conduction along the surface of the insulator and the charge decay through the bulk (decay through the volume of the bulk) [20, 21, 23-27]. The dominance of each mechanism was not yet specified, since different authors have different interpretations of ongoing processes depending on the properties of material samples (size, shape, chemical composition) as well as charging mechanism used in the experiments. Most of the surface charge decay studies so far have been limited to thin dielectric films [20, 21, 23, 24, 27-31], where the majority of the theories and models were developed in terms of electric conduction through the volume of the insulator (bulk injection). Just few studies were conducted on thick samples using different electrode arrangements and gas medium [3, 26, 32, 33].

Usually, surface potential decay measurements are performed by measuring time variations of electric potential at certain location on sample surface. Interpretation of the decay curves is the trickiest part in the analysis, since several physical processes such as sample polarization, surface

conduction, bulk injection, etc. may provide similar results. Hence, these physical phenomena should have to be clearly understood in order to get the correct interpretation of the measured results. For example, it was concluded from the experimental results [34] that the charge migration along the surface is the main decay mechanism, while other researches such as [20, 21 and 27], mostly concentrated on conduction through the bulk. Similar interpretations were also given by [22-24], with an exception that in these cases bipolar charge injection through the bulk was considered.

In [3], the potential decay on thick SIR and EPDM polymeric samples was investigated in atmospheric air at normal pressure and temperature. In this experimental work, flat materials samples and a needle-plane charging electrodes set up were used for the measurement. The sample surfaces were charged by an impulse or dc positive corona from a needle electrode placed at 1mm above the sample surface in air. The potential distribution on the sample surface (air-solid interface) was measured using a vibrating capacitive probe within 15 minutes time interval starting at 60 seconds after completing the charging. The obtained results demonstrated that of the distributions of the surface potential along the sample surface could be either of bell shape or saddle shape, depending on the magnitude of the applied voltage and the material type used (the maxima of the bell and minima of the saddle profiles were located under the charging needle). Similar results have also been reported by [23,24], in this case the simulation and experiments have been carried out on three different material samples: polytetrafluorethylen (PTFE), SIR and epoxy resin (EP) both in ambient air and in sulfur hexafluoride SF_6 - gas at room temperature and varying pressure. In [25, 38], similar electrode configurations were used, but the specimen was charged with a negative and positive dc corona of (12.5 kV) produced by a corona needle at a distance of 10 mm from the insulator surface. In the simulation work [25, 36], the authors consider three main decay mechanisms: electric conduction through the volume of the insulator, electric conduction along the surface of the insulator and the charge neutralization by gas ions, which is similar to that explained in [25, 26]. The simulations resulted in a bell shaped distribution of the surface charges, which was almost the basic shape seen in almost all the materials, and also saddle like shape distributions were obtained when neutralization by gas-ions was included. In the latter case, the decay rate was found to be faster if larger capturing volumes were considered. Hence, the atmospheric air has a great impact on the decay (neutralization) of the surface charges.

Surface potential distributions were also studied using dust figures on the samples, which were charged with an impulse and ac voltages in a point-plane electrode arrangement in atmospheric air and sulfur hexafluoride SF_6. Thus in [33], the results obtained for different dielectrics, such as Teflon (PTFE), Epoxy (filled with alumina) EP and Polyethylene (PE), showed a spread of charges associated with a bell-shaped profile for impulse voltages of lower magnitude independently on the polarity of the applied voltage. However, as the magnitude of the applied voltage increased, the potential profile was modified into a saddle-shape distribution, which is in agreement with the previously obtained results [4, 21-23, 37]. It was further noted by the authors that the surface charge decay in atmospheric air was faster as compared to the decay in SF_6. The material effect on the decay process has also been elucidated. Besides that, the faster decay on the center of the sample was explained by the contribution of the neutralization of the surface charges by charge carriers present in the gas volume above the sample surface. Similar analysis was also conducted for thin polymeric films charged by a negative corona discharge in a point-plane arrangement [20]. But in this case, the authors conclusion was that the faster decay in the central region was due to photo-injection from the surface states in to the bulk induced by the corona discharge light.

From the charge decay measurement results observed in [27], the decay of surface potential with a higher magnitude was faster than that for lower initial surface potential values. Similar experiments have been carried out by many authors, but the cross-over phenomenon was obtained only for negative corona-charged surface. In the positive corona-charging method, the cross-over phenomenon was hardly perceived [21, 22-24, 33, 41]. A significant feature of cross-over phenomenon is that the spatial distribution of the surface potential has a characteristic dip in the region where the electric field is the strongest and provides high enough energy for charges to overcome potential barrier and to penetrate through the material surface into its bulk [41]. The characteristic dip was also observed by [3, 20-24] on thin polyethylene films when charging it with negative and bipolar charges under corona discharges. The authors were able to demonstrate that the cross-over phenomena depended on the sign and the duration of the corona charging process. In their papers, it was shown that the phenomenon did not occur for positive corona voltage, which apparently contradicts the findings of [20, 21]. The effect of positive corona pulses was also studied, but no dip in the surface distribution was found [3, 21, 42]. This might be due to the additives present in the materials used [27]. But the materials used in [20, 21] were untreated and additive free.

When considering the charge transport in insulators, it is crucial to select proper transport model and parameters to be used in order to describe the phenomena seen through the externally measured quantities. Generally speaking, there is great number of charge transport parameters governing charge decay, which are related to corona charging conditions (grid voltage, charging time), sample thickness, charge carrier trapping rates, diffusion, mobility, partial instantaneous charge injection, etc. Most of them are field dependent that makes the problem to be strongly non-linear. In the theoretical analysis done in [3, 24], some simplifications were introduced, e.g., general expressions were derived by fitting different material parameters, such as field dependent mobilities of charge carriers as well as trapping and injection rates. Similar studies in [34] and [41] suggested more complex models for the processes involved. However, simulations for charge decay are still far from been able to explain all experimentally observer features and they are the subject of ongoing research.

Most of the models and experimental works carried out for investigating the charge dynamics in dielectric materials were done by considering plane samples of certain thickness *d* resting on a grounded plate with its upper surface charged up to an initial potential V_0 as depicted in Figure 2.3. Under such conditions, one may expect that the charges on the surface are located in a very thin slab with thickness *a*. As it was pointed out in [52], the charge does not move as a thin sheet through the insulator but spreads out during the movement through the material. Due to the charge distribution located in a limited area, the charges introduce

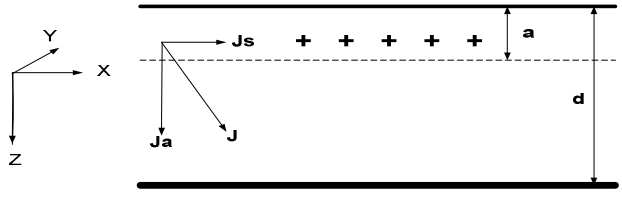

Figure.2.3. Schematic of a plane insulator with charged surface represented as a thin charged slab of material.[1]

potential gradients on the surface and in the bulk, which means that some of the charges are transported along the surface and some charges are transported through the bulk of the material. Consequently the mechanisms that will control the charge dynamics depend on geometrical structure of the system, electric field distribution and other relevant factors.

2.3. Effect of surface charges on flashover performance of polymeric materials

The application of polymeric insulators as an outdoor insulation has been increased the last decades especially with the upgrading of the HVDC transmission capacity. Hence, the efficiency or withstand performance of the insulators should be increased in order to insure reliability of the insulation system. Although withstand performance of polymeric materials has been studied for several years, there is still a lack of a comprehensive physical understanding, particularly there is a lack of knowledge of the surface flashover mechanism in polymeric material surfaces. Hence the presence of surface charges on polymeric material surfaces and their effect on the flashover mechanism should be deeply considered when designing high voltage insulators and performing insulation coordination especially for high voltage dc application where the presence of the surface charges is an inherent property of the system.

In the experimental investigations which were done on real samples [35], prototype insulators [37, 38 and 40] and on material samples [36], it was found that the flashover voltage is strongly affected by the presence of pre-deposited surface charges. In [35], variations of $U_{50\%}$ lightning impulse flashover voltages (FOV) due to the pre-deposited charges on a 15kV high density polyethylene (DPE) insulator were studied by considering three different wetting conditions: dry, semi wet and heavy wet. The author observed a significant reduction of the impulse flashover voltages due to wetting and concluded that the presence of surface charges under negative impulse application led to increases in the flashover voltages. Similar results were reported in [36] where the experiment was conducted on SIR and EPDM material samples under normal temperature and pressure. The authors demonstrated that deposition of negative charges resulted in an increase of the FOV while positive charges reduced the $U_{50\%}$ FOV characteristics under an impulse voltage application. These were dependent on the polarity of the applied impulse voltage. Thus when the polarity of the deposited surface charges were the same as that of the applied LI voltage, the FOV was reduced for positive polarities and the opposite was true for the negative polarity. But when the deposited charges had an opposite polarity to the applied LI voltage, positive charge in combination with the negative LI resulted in a decrease of FOVs while negative charges in combination with positive LI led to considerably higher FOVs. It is notable [36] that presence of ATH filler in the insulator material provided higher flashover voltages as compared to pure material. This effect was more pronounced for SIR. The experimental results were reported in [40], where insulated conductors covered with thick (3 mm) XLPE were utilized, demonstrated an increase of $U_{50\%}$ due to deposited surface charges.

Many investigations have also been done on prototype polymeric materials related to SF_6-filled gas insulated systems GIS [37-39]. In [37], particle contaminated spacer made of an aromatic epoxy resin type (with diameter and height of 40mm) was placed in SF_6 gas under atmospheric pressure of 0.1 MPa. The tests were done with standard lightning impulse (1.2/50μs) voltages. It was found that the flashover voltage was seen to increase or decrease depending on the polarity of the applied surface charges. For example, when positive surface charges were deposited on the spacer, the

lightning impulse withstand voltage increased by about 40kV that should be compared with 80 kV FOV measured for the charge-free spacer. For negative deposited surface charges, the FOV has decreased for about 30kV even with higher amount of charges imposed on the surface. In [38, 39], cylindrical PTFE insulators of diameter 20 mm and height 10 mm with a particle contaminated surface located at the anode or in the middle of the sample were tested at 1.0 bar SF_6 pressure. In this case, the effect of charge deposition was qualitatively similar to that observed in [37]. It was concluded also that the flashover characteristics were dependent not only on the polarity of the deposited charges and the applied LI voltages, but also on the magnitude of the LI voltage and the distribution of the surface charges.

CHAPTER 3

3. EXPERIMENT ON CHARGING MECHANISMS

3.1. Physical background

This chapter focuses on experimental analysis of different charging mechanisms of polymeric material surfaces, namely by an impulse voltage application and by discharges in air under dc corona. The first method was utilized (a) to see if the surface of polymeric materials can retain charges after application of short energizing pulses, and (b) to see if the retained or deposited charges under the impulse stress have an effect on the flashover voltage performance. As it was reported in [19, 35-40], the application of lightning impulses to polymeric insulating materials, including composite insulators, may result in deposition of significant quantities of charges on sample surfaces leading to a "memory effect". That means that preceding impulses may affect the flashover voltages of polymeric insulators. The standard measurements of FOV characteristics, which has been practiced for several decades on ceramic insulators, is a statistically independent test meaning that $U_{50\%}$ FOVs are statistically repeatable and can be obtained by some standard methods such as up-and-down method, multi-level test method, extended up-and-down method, etc[50]. For polymeric materials, the tests procedures based on the mentioned methods often provide ambiguous results, presumably due to influence of charges accumulated during impulse voltage applications preceding flashovers.

Surface potential distributions along the surface of polymeric insulators associated with the charging were measured using a capacitive probe and electrostatic voltmeter. In the first series of tests, the dielectric samples were initially stressed by lightning impulses from an impulse generator (Haefely, 800kV, 24MW). In the second part of the study, charge decay processes and the effect of deposited surface charges on the $U_{50\%}$ FOV characteristics was investigated on SIR and RTV-SIR material samples charged with direct current (dc) corona discharge. The objective of the second part is to deposit higher amount of charges on the surface of the polymeric samples. In both cases, the influence of the accumulated charges on the $U_{50\%}$ lightning impulse FOV has been investigated. All the experimental tests were done in a high voltage laboratory at Chalmers University of Technology.

The material properties, and the methodology used for charging mechanism, the decay process and the flashover results in the presence of surface charges will be treated in detail here and in the next chapter consequently.

Material properties

The materials used in this study were cylindrical samples of SIR and RTV-SIR (in the latter case it was a 2 mm layer covering a ceramic rod) of 30 mm diameter and 114 mm length, as can be seen from the Figure 3.1. Materials formulations were according to Elastosil R401/50(Wacker Chemie, Germany) and contained PDMS and approximately 20 wt.% of

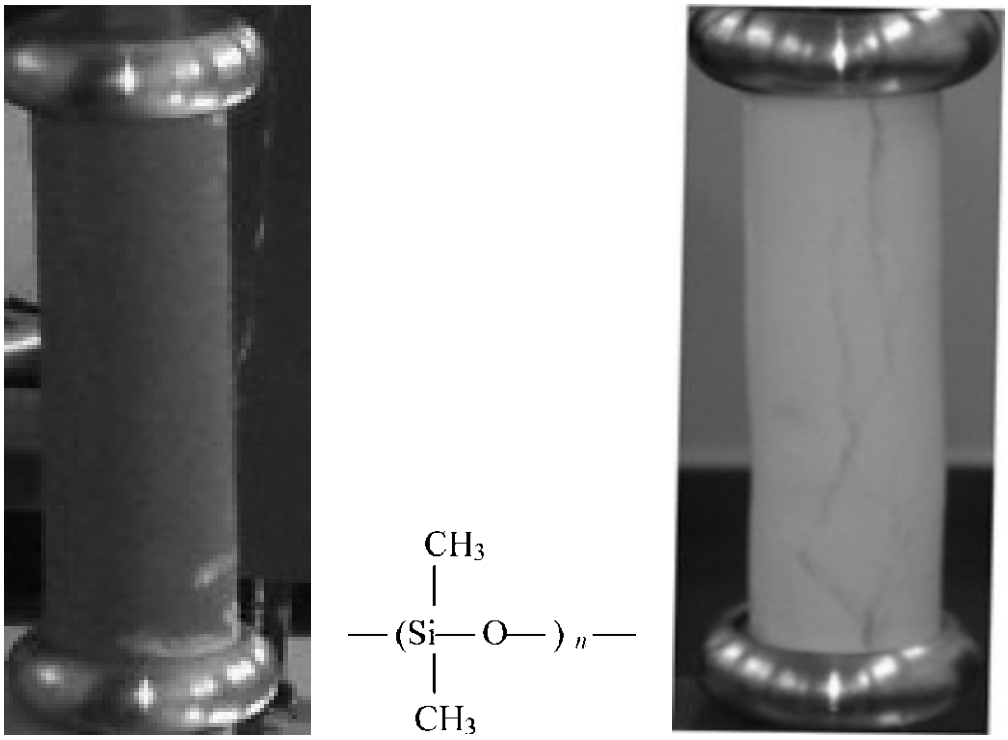

(A) *Molecular structure of PDMS* (B)

Figure 3.1. The sample insulators: (A) RTV-SIR and (B) SIR

reinforcing silica filler. The ATH added was alumina hydroxide $Al(OH)_3$ (Martinal OL-104/S from Martinwerk, Germany). The filler particles were silanized and had a geometrical form of pseudo-hexagonal platelets, and a particle size distribution in which 10, 50 and 90 we.% of the particles have a smaller diameter than: d_{10}:0.5 to 0.8 μm, d_{50}:1.3 to 2.2 μm and d_{90}:2.2 to 5 μm. Further details on materials properties and chemical compositions can be found in [41]. According to [43], the resistivity value for the SIR materials was ~$10^{12}\Omega$m and the relative permittivity for the SIR was 3.5 whereas the RTV-SIR polymeric materials it was 3.2.

3.2. Charging of polymeric samples by an impulse voltage

3.2.1. Experiment set-up-I

The experimental set-up for the charging of SIR and RTV-SIR covered ceramic materials using a standard LI voltage stress is illustrated in Figure 3.2. The set-up consists of cylindrical SIR or RTV-SIR samples placed between two stainless-steel electrodes with Rogowski -profile. A standard impulse voltage generator (Haefely, 800 kV, 24kJ) was used. During the experiment period, only three stages of the impulse generator were utilized. The impulse shape was 1.2 (±30%) / 50 (±20%) µs through the whole work. The impulse high voltage was down scaled to a measurable value via the high voltage divider (damped capacitive voltage divider) with the equivalent capacitance of HV-site of C1=1416 pF and resistor R1= 80 Ω. The low voltage site was composed of a capacitor C2=1.0381µF and the low voltage resistor

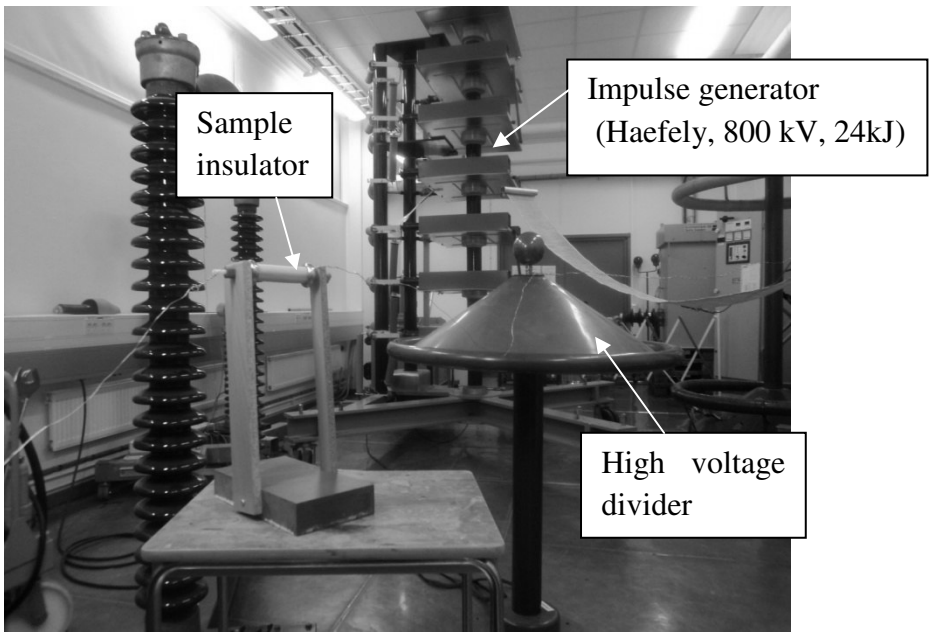

Figure 3.2.The experimental set-up for a lightning impulse voltage stressed SIR and RTV-SIR materials under normal temperature and pressure

of magnitude of 75 Ω. Details of the experimental methodologies used are explicitly defined in the charging procedures below.

3.2.2. Charging procedure-I

As it was previously mentioned, the samples used here were pre-stressed by impulse voltages of magnitude lower than the FOV level. The charging voltage and the number of applied impulses were varied.

Just before and after the start of the experiment, the samples were cleaned with isopropyl alcohol and dried so that they could be considered free of charges. The removal of surface charges along the samples was also cross-checked by scanning with a capacitive probe connected to the electrostatic voltmeter.

During the flashover test, one of the metallic electrodes was grounded and the other electrode was connected to the high voltage source. The measured FOV was then monitored in a computer for an accurate interpretation and documentation.

Finally, the $U_{50\%}$ of the LI FOV was investigated using the up-and-down method and the obtained values were used as a reference and sequences of impulses were applied to the polymeric samples. Since each flashover should be independent on charges remained from the previous one, charge was carefully neutralized before and after every impulse application. First the sample was discharged through contact with a ground copper foil. The surface was then cleaned using a soft paper soaked with isopropyl alcohol. The effectiveness of charge removal was also again checked with an electrostatic voltmeter (Trek-523), a device which was designed to measure electrostatic surface voltages from 0 to $\pm$20kV with the ground snap

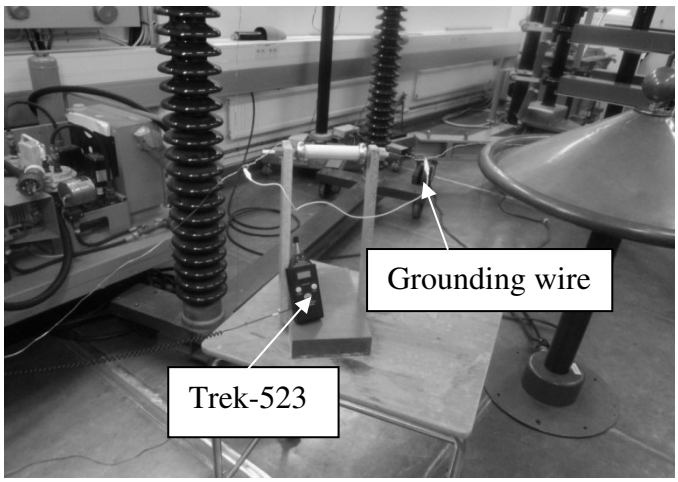

Figure 3.3. Measurement of potential on sample surface

connected to the ground reference point using the cable provided as can be seen from the Figure 3.3.

The above measurement gave a rough estimation of the surface flashover voltage(FOV) on a clean surface. Next, charge accumulation was studied when a sequence of impulses at a level of about (0.7-0.8) $U_{50\%}$was applied. After each impulse, the surface potential was measured. It was experimentally observed that an impulse forms a charge of the same polarity as that of the applied voltage. This is in agreement with findings reported in [35, 36]. To study the effect of charged surface on the flashover voltage, a sequence of successively increasing LI voltages starting from (0.7-0.8)$U_{50\%}$ was applied until flashover occurred. The voltage level of each applied impulse was increased by approximately 3kV.

The FOV was also investigated when the surface was charged to the opposite polarity as compared to the applied impulse polarity. In this test, three impulses were first applied to deposit charge on the polymeric surfaces. Then, an impulse of the opposite polarity was applied. The voltage level of the first applied impulse of opposite polarity was (0.7-0.8)$U_{50\%}$ as previously stated, and if a breakdown didn't occur, three impulses at a level of (0.7-0.8)$U_{50\%}$ were applied to charge the surface again. Now, another impulse of opposite polarity was applied at the voltage level increased with steps of about 3 kV. This procedure was repeated until a flashover occurred. Similar test procedure was adopted in [36] on a needle-plane electrode arrangement on flat SIR and EPDM polymeric samples.

3.3. Charging of polymeric surfaces by a dc-corona discharge and procedures

Corona is a discharge that appears when the electric field on the surface of the discharge electrode is greater than the ionization threshold of the surrounding gas medium. This mechanism generates an excessive amount of free charges in the neutral gas volume. It was ascertained in a number of investigations, that corona charging is the most effective method of charging polymeric material surfaces, hence it was adopted in this experimental work.

The corona charging electrode set-up used in this study is illustrated in the Figure 3.4 below.

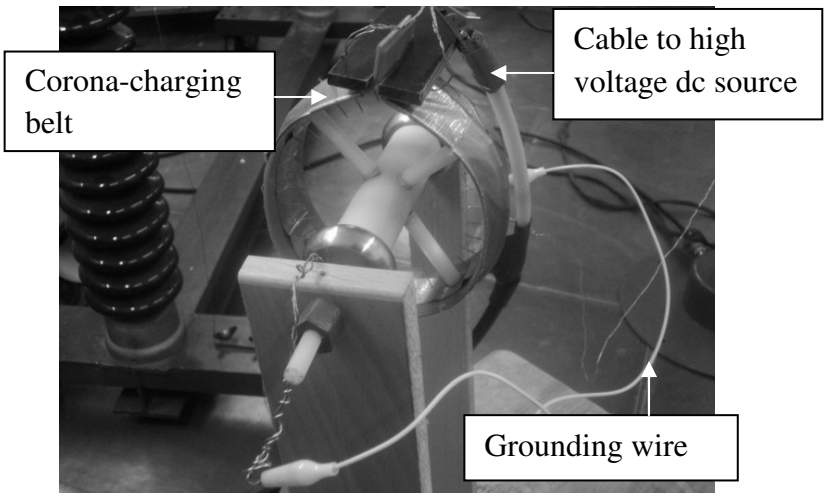

Figure 3.4. The electrode arrangement for corona charging

As it can be observed, the corona source was a circular belt placed on the center of the cylindrical dielectric samples (can be termed as a point electrode-convex surface arrangement). The corona belt contained 30 conical stainless-steel needless of length 21 mm with tips radius of about 50μm. The corona charging needles were placed 10 mm apart from each other in order to achieve a nearly homogeneous electric field distribution in the vicinity of the treated surface. Each needle pointed normally to the insulator surface. The diameter of the charging belt was 112 mm and it was supported by four plastic legs of lengths 41 mm, each ending with a flat 0.5 mm thick silicon rubber disk glued under each of the supports. The disks were used in order to reduce the contact friction between the sample surface and the support legs.

During charging, both ends of the sample were grounded (white connecting wires seen in the figure) and all the corona-needles were connected to a high voltage dc source. The corona belt provided a symmetrical ring-type distribution of charges on the dielectric surface. It should be noted here that the corona-charging belt was placed at the center of the sample materials throughout the whole study.

After charging, the corona belt was quickly removed and the sample's surface was scanned using a vibrating capacitive probe, which measured the potential of the surface being studied. The probe was of high resolution and during scanning it was located in close vicinity (2mm) to the treated surface to achieve accurate measured results. The probe was connected to an electrostatic voltmeter (either Trek 347 or Trek 341B models). The obtained signals were down scaled in magnitude to a value which could be handled by a BNC-211 adapter and monitored in a computer using an analog/digital (A/D) controller to the data acquisition card. The surface potential was then measured and continuously recorded. A schematic diagram that illustrates the measuring circuit can be seen in Figure 3.5.

Since the surface potential measurement depends on the experimental charging conditions such as temperature, the relative humidity and charging duration, the experiments were carried out at normal temperature and pressure. Before each experiment test, the magnitudes of the temperature and pressure were recorded. The charging duration was 120 s throughout the whole work.

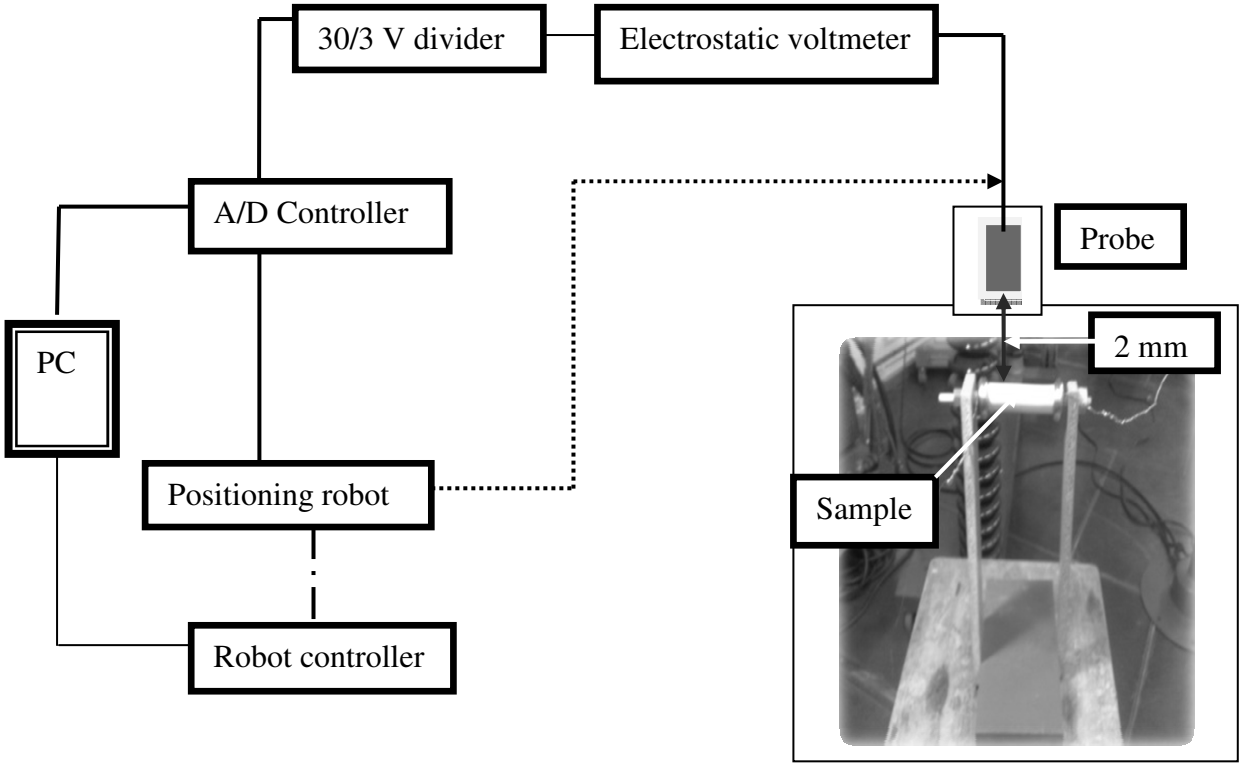

Figure 3.5 .Schematic view of the potential measurement on a corona charged surface

3.4. Results of the potential distribution and decay measurements along an impulse pre-stressed and dc-corona charged polymeric samples

Initially, the FO voltage tests were done on a clean SIR and RTV-SIR material surfaces according to the steps outlined in the procedure-I above. This study was intended to provide reference values for the applied pre-FOV impulses used to deposit charges on sample surfaces.

The measured surface potentials appeared due to application of impulse voltages of magnitude lower (about 80%) than the FOV to the sample insulators can be seen in Figure 3.6. The results shown present the withstand voltages (light green-color), flashover voltages (black dots) as well as the magnitudes and polarity of the potentials due to deposited charges along the dielectric surfaces (red-color).

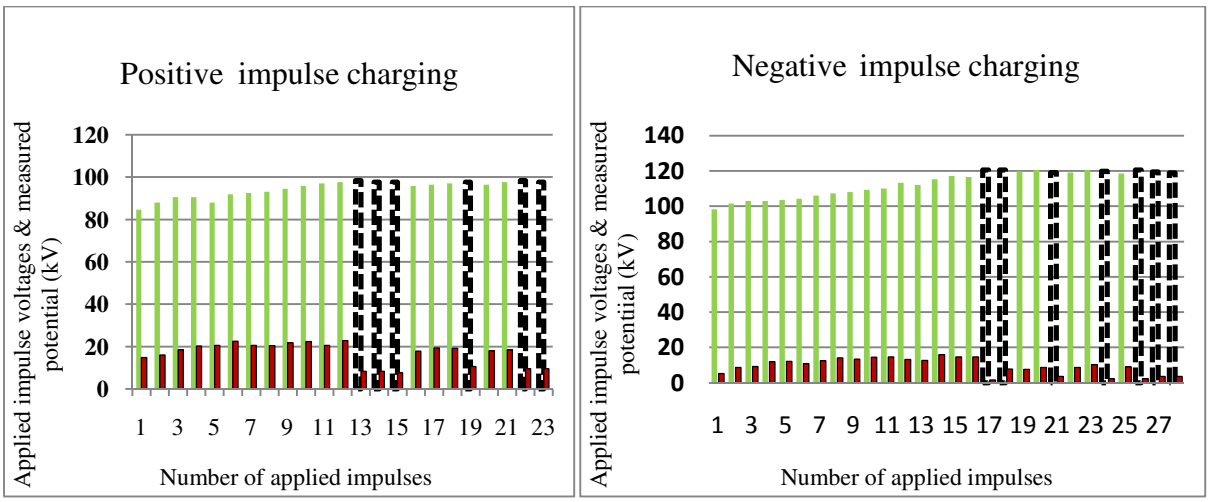

(a)

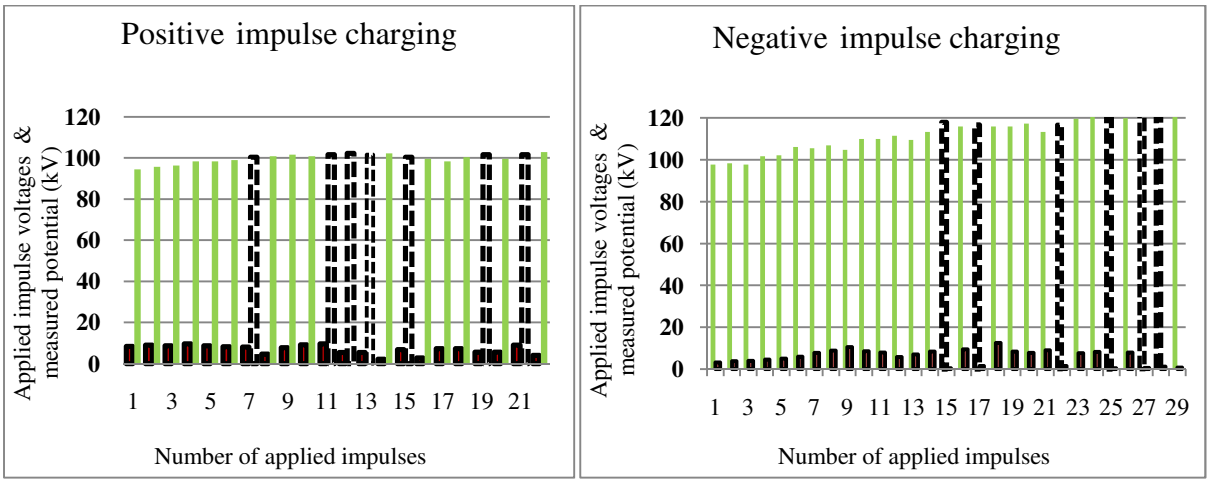

(b)

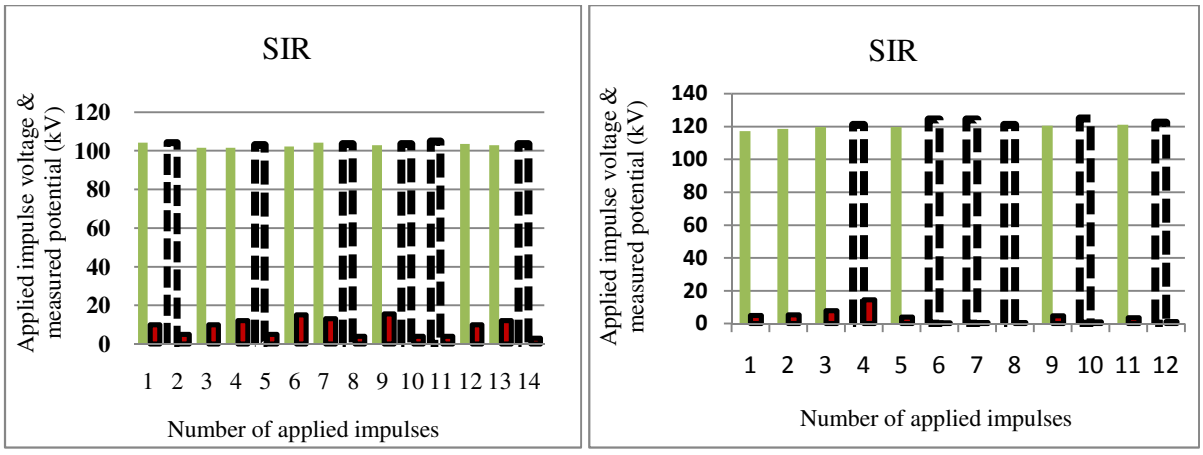

(c) *(d)*

Figure 3.6. Results of the measurements with LI voltage pre-stressing: (a) uncleaned SIR insulator surface; (b) uncleaned RTV-SIR; (c) applied positive impulse on a negatively pre-stressed sample; (d) applied negative impulse on a positively pre-stressed sample. Legend: *Measured withstand voltages,* *measured FO voltages, and* *Potential due to deposited surface charges.*

3.4.1. Surface potential distribution on LI pre-stressed samples

As can be seen from Figure 3.6, the polarity of the deposited charges (homocharges) was found to be the same as that of the applied impulse voltage. The surface potential (deposited charges) due to pre-stressing was the highest closer to the high voltage electrode side and decreases towords the grounded electrode side. These accumulated charges on the samples surface were also slightly higher for negatively impulse voltage than for the positive applied impulses. The results demonstrated that charges could be deposited on the dielectric surfaces by preceding voltage impulses, but the recorded magnitudes of the induced surface potentials were very low. These are illustrated in Figure 3.6 (a)-(d) with red colored bars the height of which is magnified by factor 20 to make the potential visible on the diagram. Hence, one may conclude from the presented results that the effect of pre-stressing with impulse voltages was weak under the conditions of the present investigations.

3.4.2. Surface potential distribution and decay on a dc-corona charged samples

The electrode set-up used for corona-charging is presented in Figure 3.4 above. Before charging, the polymeric samples were cleaned with isopropyl alcohol and dried so that they can be considered initially free of charges. Then, the sample surfaces were charged by dc corona-discharge. A Spellman (±33kV, 6 kW rated voltage and power, respectively) high voltage dc power supply was used. The arrangement allowed to deposit uniformly distributed charges with polarity corresponding to the HV applied impulse (homocharges) or of opposite polarity (heterocharge).

The dc corona was applied for a time period of 2 min with the corona charging belt placed in the center of the sample surface for the chosen voltage level. Four different voltage levels of both polarities have been tested: ±5kV, ±10kV, ±15kV and ±20 kV. During charging, both ends of the samples electrodes were grounded to ensure a proportional (symmetrical) surface potential. A number of tests have been conducted for each voltage level in order to select the repetitive (appropriate) charging voltage. All tests were carried out at normal temperature (23℃) and pressure 1.01 MPa in atmospheric air. This was done to provide a comparison of these experiment results with the real implemented outdoor polymeric insulators. Then the temporal and spatial distribution of potential along the samples surface was measured using the vibrating probe.

The probe was calibrated before measurements by scanning a metal surface subjected to a variable dc voltage. In the experiments with the samples, the probe's movement along the treated surface was done using a robot (Arrick Robotics), which can be directed in both X and Y directions. The robot was positioned on a table which made it easier to move in both directions and minimize the vibration. The positioning table was connected to MD-2 stepper motor controller which was coupled to a personal computer to help the user to have a complete control over its movement. The sample surface was scanned three times (even more in some cases) for each voltage level. The charging voltages for further FOV measurements were chosen to be 20 kV and -15 kV for positive and negative dc corona charging, respectively, which provided similar total currents of the corona discharge. To discharge the dielectric samples between tests, the surface was cleaned before and after every test with a cloth soaked with isopropyl alcohol. It was also rechecked by the vibrating capacitive probe. It should be noted that the measurement process for the RTV-SIR dielectric material was started 1 minute after the completion of the charging process for both polarities. For

the SIR material, the measurement process was started 3 minutes (stability monitoring time) after charging. This delay time in SIR material was chosen due to the fluctuations of the readings before the specified time and due to the fact that the loss of deposited surface charges was relatively slower.

Surface potential distribution on dc-corona charged samples

The preliminary analysis was done on the measuring the spatial distributions of the potential along the surface of the dielectric samples. The measurement results obtained for each voltage level of both polarities are outlined in Figures 3.7 and 3.8. The plots of figure 3.7 represent the surface potential profiles for positively charged SIR sample and the plots of Figures 3.8 (a)-(d) show the distributions of the surface potential for negatively dc-corona charged SIR samples.

As it can be seen, the magnitudes of the potential increases with the applied corona charging voltages in both polarities and the potential profiles are more symmetrical at higher charging levels. The measured distributions showed both bell and saddle like profiles for the selected voltage levels for positively charged insulator while negative corona led to the bell-shaped potentials.

One should note here that the flat regions observed in Figures 3.7(d) and Figure 3.8 (c) and (d) appeared due to saturation of one of the probes used in the measurements (Trek- 347B, measures surface potentials up to 3kV). To avoid this problem, another probe (Trek 341B measures surface potentials up to 20 kV) was used in the rest of the experiments.

From the preliminary experimental study, the levels of +20 kV and -15 kV were chosen as charging voltages to be used for the FOV tests on corona charged insulators. At these voltages, the charging current was ~0.1 mA. The corresponding charging conditions and resulted surface potential profiles were examined in details to secure their repeatability.

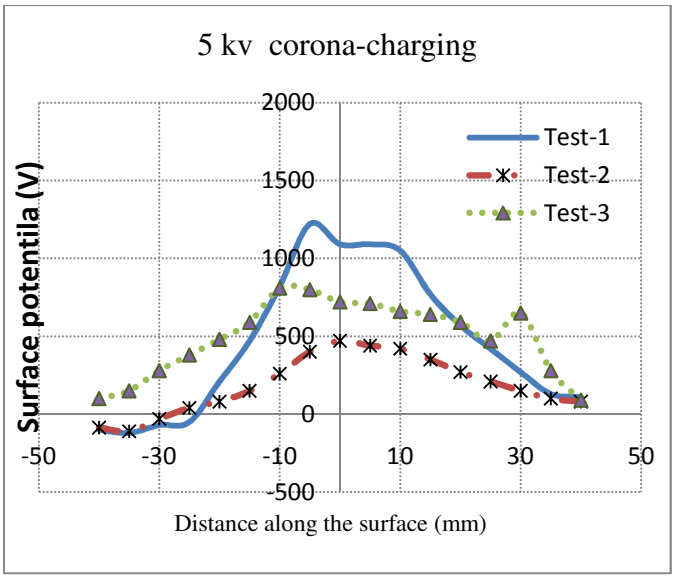

(a)

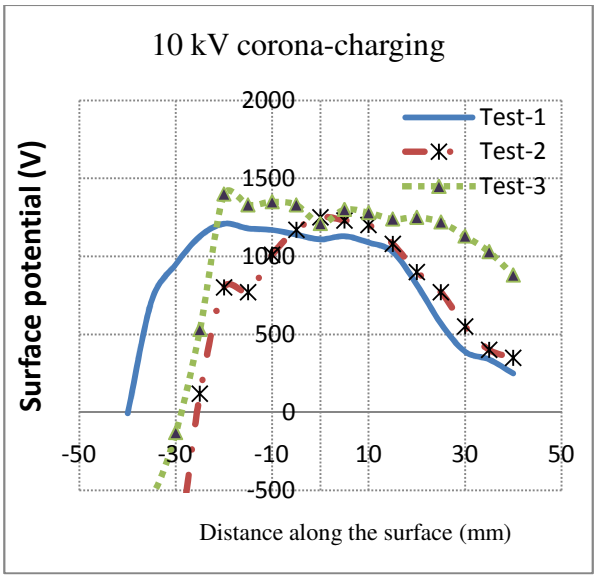

(b)

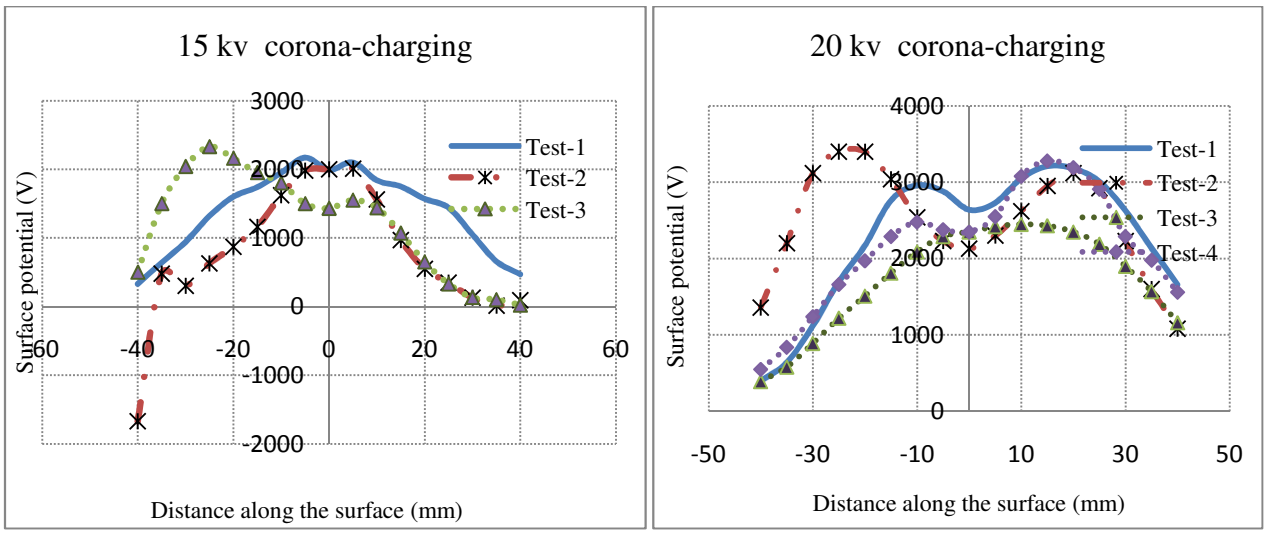

(c) *(d)*

Figure 3.7. Measured surface potential distributions (V) along SIR sample charged by positive dc corona for four different voltage levels.

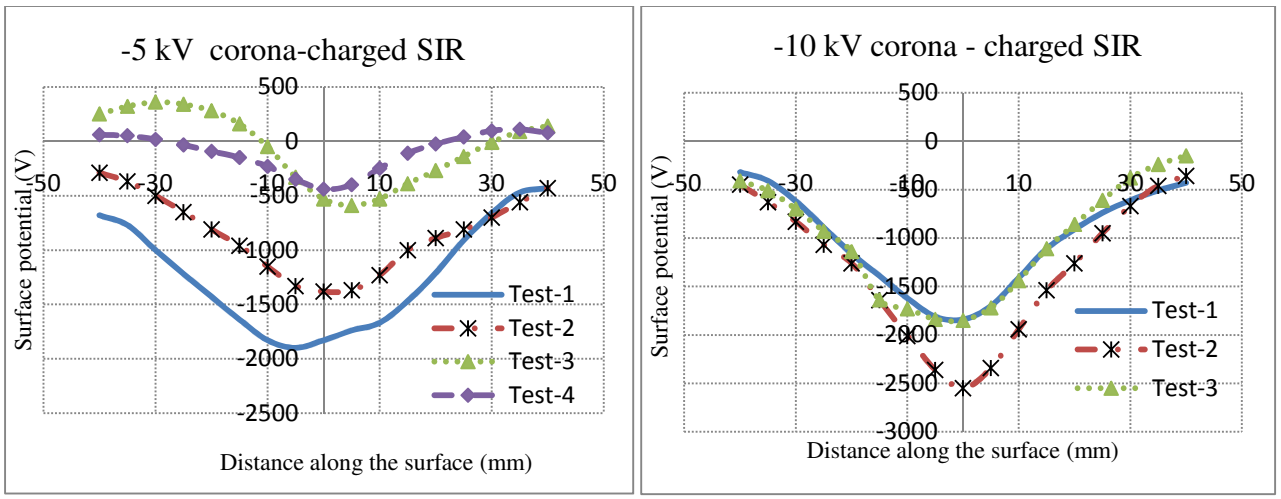

(a) *(b)*

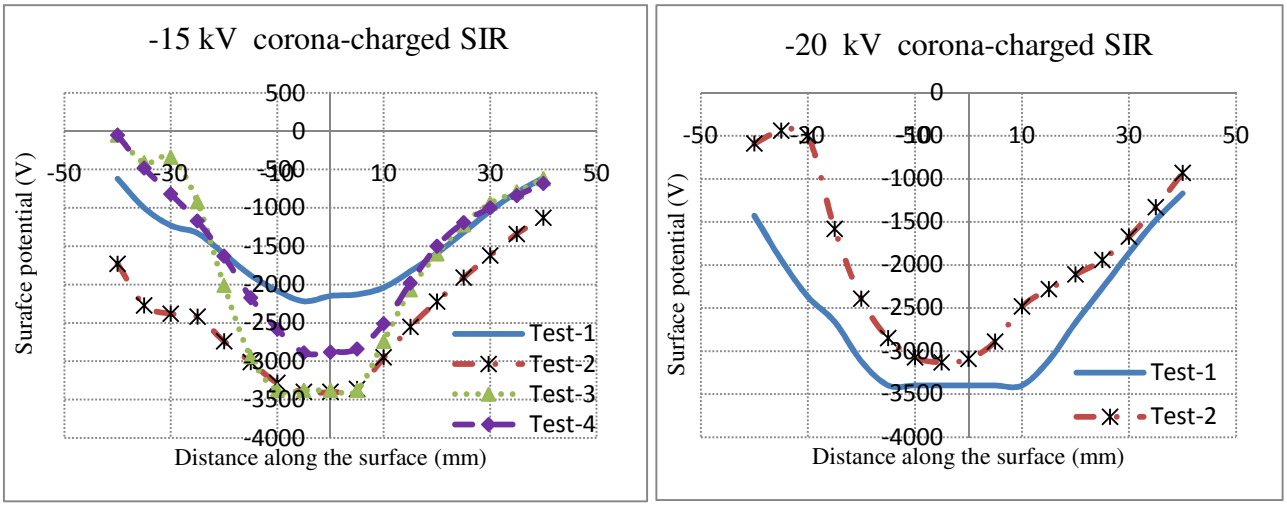

(c) *(d)*

Figure 3.8.Measured surface potential distributions (V) along SIR sample surface due to charging by negative dc corona for four different voltage levels.

The time variations of the surface potential distributions along the sample charged by applying +20 kV are presented in the Figures 3.9 and 3.10 for SIR material. The measured distributions on RTV-SIR materials are shown in Figures 3.11 and 3.12. Note that the plots in both Figures 3.10 and 3.12 illustrate the cumulative and averaged potential distributions, respectively. The measured time variations of the surface potential distributions and their averaged dynamics on negatively charged surfaces of RTV-SIR samples are presented in Figure 3.13 and 3.14.

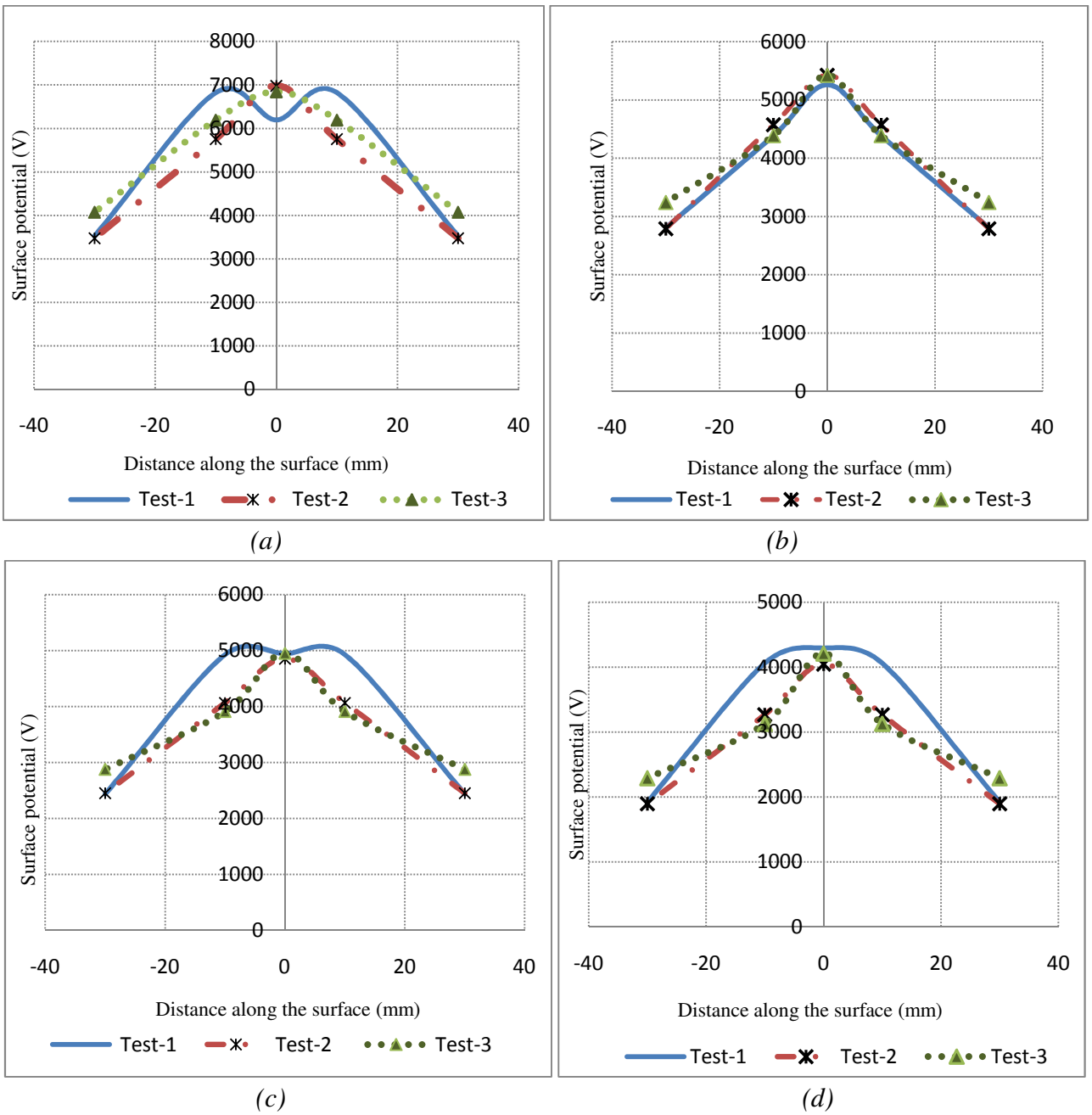

Figure.3.9. Measured surface potential distributions along positively corona-charged SIR sample surface at four different time instants: 1min (a), 2min (b), 3 min (c) and 5 min (d).

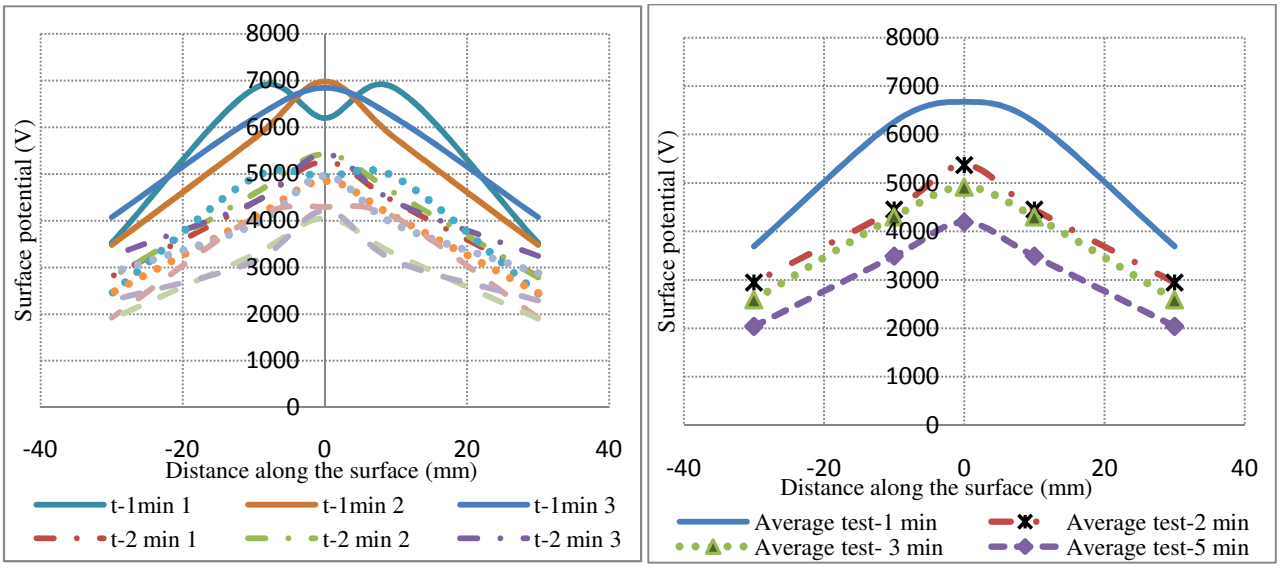

(a) *(b)*

Figure 3.10. The cumulative (a) and averaged (b) surface potential distribution on a positively charged SIR sample surface.

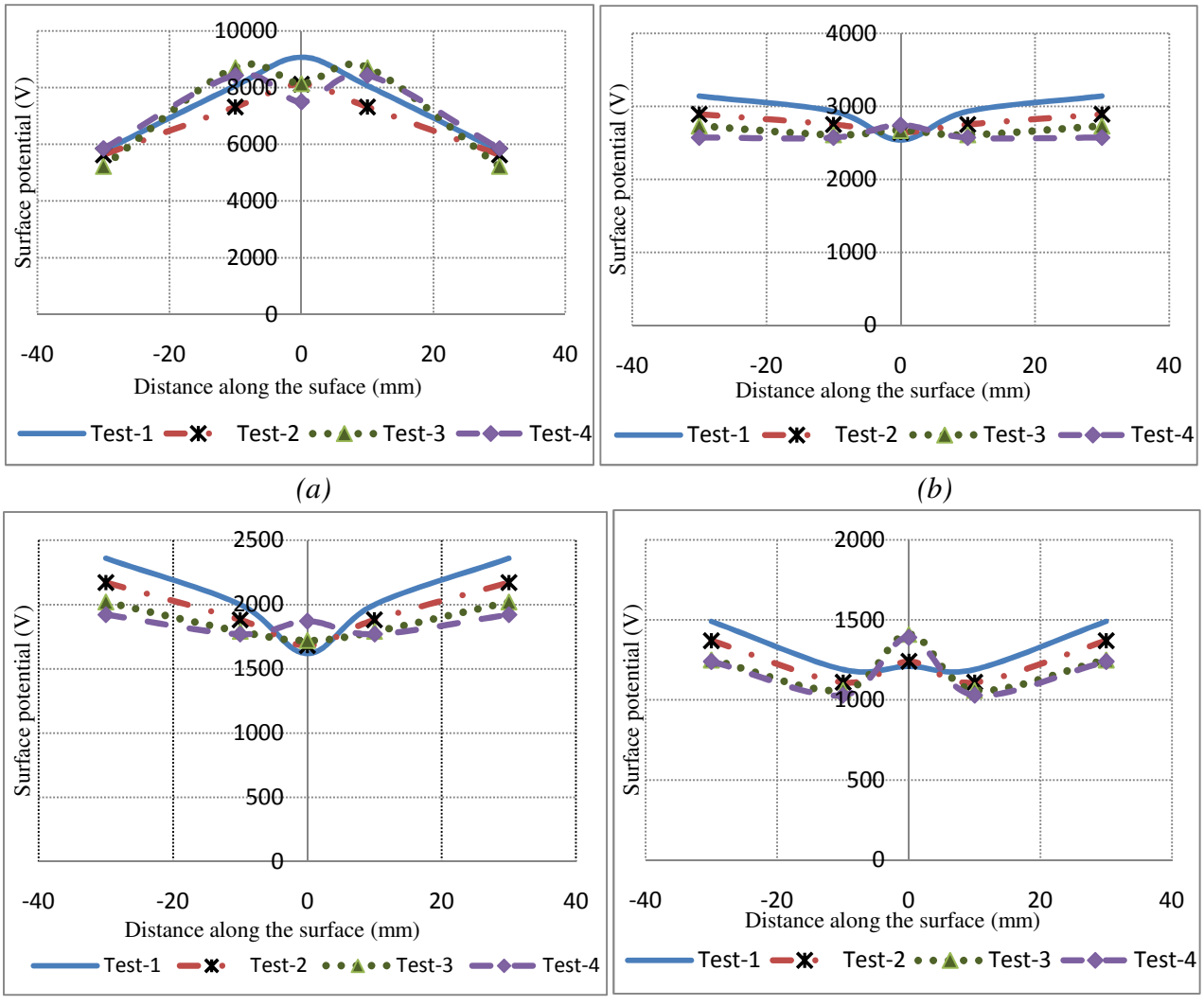

(a) *(b)*

(c) *(d)*

Figure.3.11. Measured surface potential distributions along positively corona-charged RTV-SIR sample surface at four different time instants: 1min (a), 2min (b), 3 min (c) and 5 min (d).

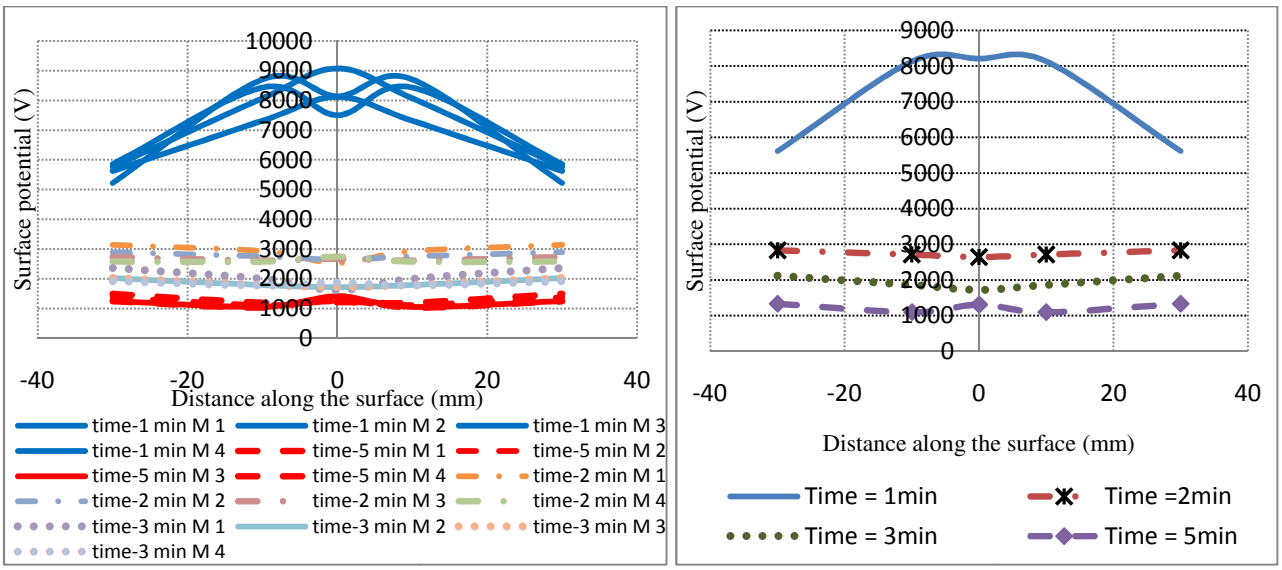

(a) *(b)*

Figure 3.12. The cumulative (a) and averaged (b) surface potential distribution on positively charged RTV-SIR sample surface.

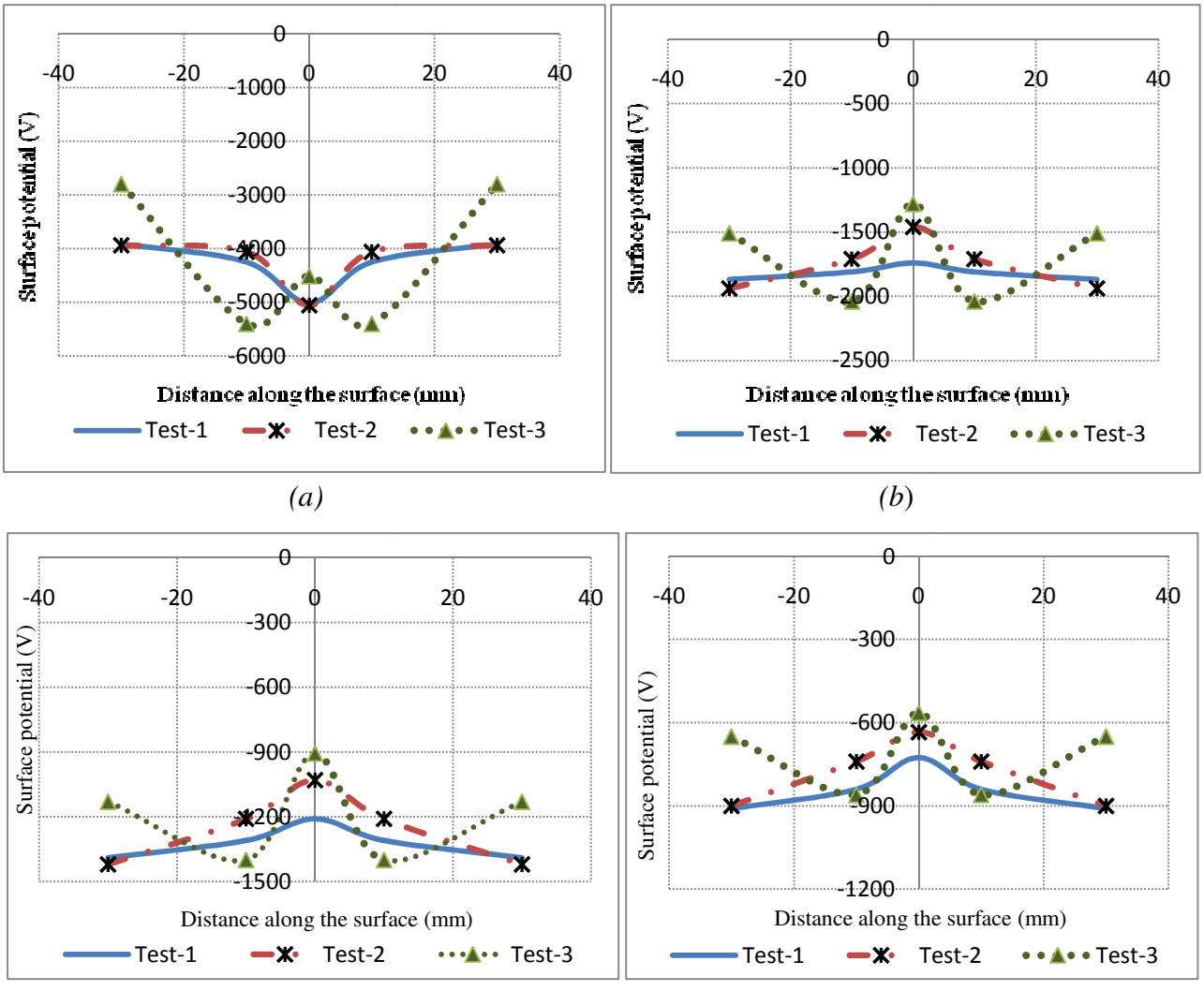

(a) *(b)*

(c) *(d)*

Figure.3.13. Measured surface potential distributions along negatively corona-charged RTV-SIR sample surface at four different time instants: 1min (a), 2min (b), 3 min (c) and 5 min (d).

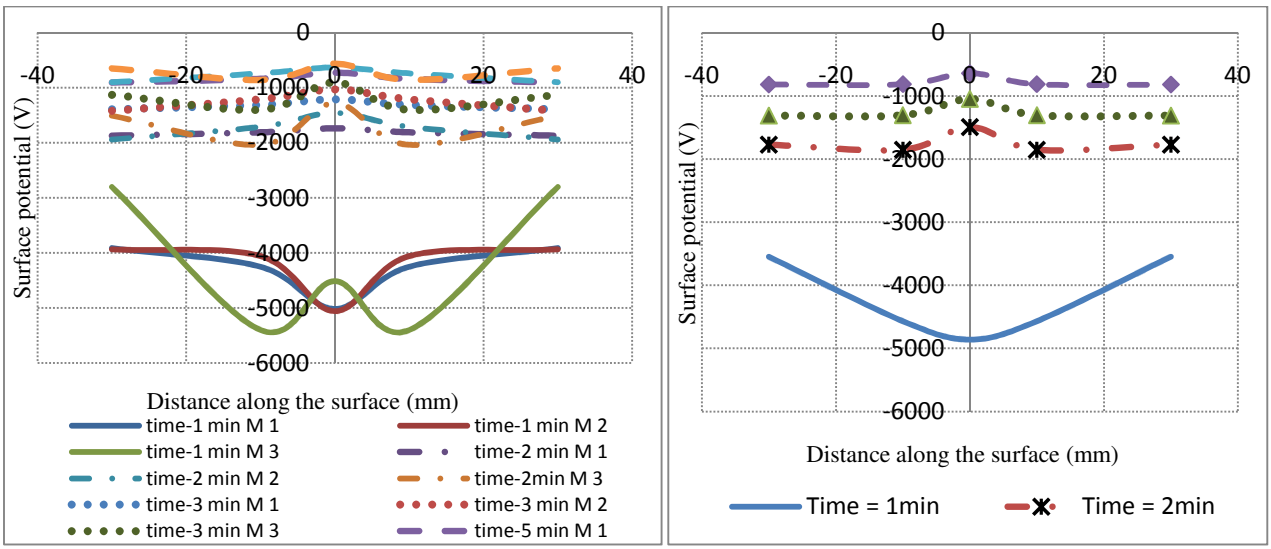

(a) *(b)*

Figure 3.14. The cumulative (a) and averaged (b) surface potential distributions on negatively charged RTV-SIR sample surface.

As it can be observed from the Figures (3.9-3.14) above, the potential distribution along the treated materials surfaces showed both bell and saddle like distribution over the selected voltage levels. In case of the saddle like distribution for the positive corona charged SIR sample, the potential at the center of the sample is lower and it increases towards the end electrodes this may associated with the geometry of the charging arrangement. Since the charging belt was located at the center of the samples hence, the contribution of the neutralization of the surface charges by charge carriers present in the gas volume above the sample surface can lead to a loss of more charges from the center of the treated samples. Similar shapes have also been determined for the negative corona charged samples as well. But one can see that the measured potential profiles were not symmetrical as expected, for example the temporal and spatial distributions of potential along SIR and RTV-SIR samples surfaces of Figures 3.10 and 3.14 differs significantly. This might be associated with the differences in surface conductivities of the materials and the simultaneous decay processes happening during and after charging. The different material compositions and additive used which in turn leads to a difference in properties should also be considered; since it affects the electric field distribution along the surface of the materials. In case of the RTV-SIR materials the magnitude of the measured potential was higher than that of the SIR material samples, this might be due to the properties of the utilized material and the RTV-SIR samples had small (about 10 mm in length) metallic threads put in wards in both ends, hence these might affect the field distribution and change the surface potential profiles. Other factors can be related to the presence of surface defects on the material samples. The physical smoothness of the two samples was not the same, because the RTV-SIR samples were a bit rougher than the SIR materials, and this may lead to trapping (accumulation) of more charges on the RTV-SIR material surface, as a result it can lead to a higher effect on measured surface potential along the samples.

Finally it can be said that there was no significant difference of the potential distribution profiles between the positively and negatively dc-corona charged RTV-SIR samples. The only difference observed was the magnitudes and this was due to the magnitude of the applied dc corona charging, as it was explained above. Similar characteristics were also seen for the SIR materials.

Surface potential decay on a dc-corona charged samples

The decay of the surface potentials measured on the samples surfaces directly below the corona charging needles for SIR and RTV-SIR are shown in Figures 3.15 (for a positively charged materials) and 3.16 (for a negatively corona charged samples), respectively. The decay measurement has been carried out for 20 minutes because the magnitudes of the surface potentials obtained on RTV-SIR samples was found to be too low after the considered time period. Hence, for the sake of comparison of the decay rates among the two materials, the time frame was marginalized to 20 minutes. From the decay measurement results shown one can relate the rate of decay to the measured surface potentials. From the plots of figures 3.15 (a), (b) and (c), for positively dc-corona charged SIR and RTV-SIR materials, it was found that the magnitude of the measured surface potential was higher (about 9 kV) on RTV-SIR surface, while it was about 6.5 kV on SIR samples. Similarly, the decay rate on RTV-SIR samples was higher about 3 kV/min, but for the SIR sample materials it was found to be 1 kV/min. It should be noted that the applied dc corona charging voltage levels, charging time and gas medium used for both materials were the same and the corona charging belt (with corona needles in it) was located in the center of the sample surface. From these results one can observe that the material properties have a significant influence on the potential decay.

The fast decay process in the beginning of the decay measurement can be associated with the simultaneous occurrence of different mechanisms such as the loss of surface potential due to surface conduction, charge injection (transport) through the volume and neutralization of the deposited charged by the charge carriers present in the surrounding gas medium. It was explained by different authors that the dominance of these processes in not yet verified. But for the conditions of the present experiments, the charge neutralization by gas ions may be suggested as the dominant mechanism due to high resistivity of the materials used and negligible lateral expansion of the measured potential profiles (see previous chapter). Moreover, injection to the material bulk seems to be not important at all due to the dominant influence of the tangential (to the insulator surface) component of the electric field in the considered electrode arrangement. Hence, the deposited charges do not have enough energy to be injected into the polymeric samples.

Note that for the positively charged SIR and RTV-SIR material samples, the potential decay measurements were carried at three different positions along the sample surface, Figure 3.15(c), and the obtained decay rates (the slopes of the curves) were similar throughout the samples surface even the magnitudes of the potentials can be different. This issue requires more investigations.

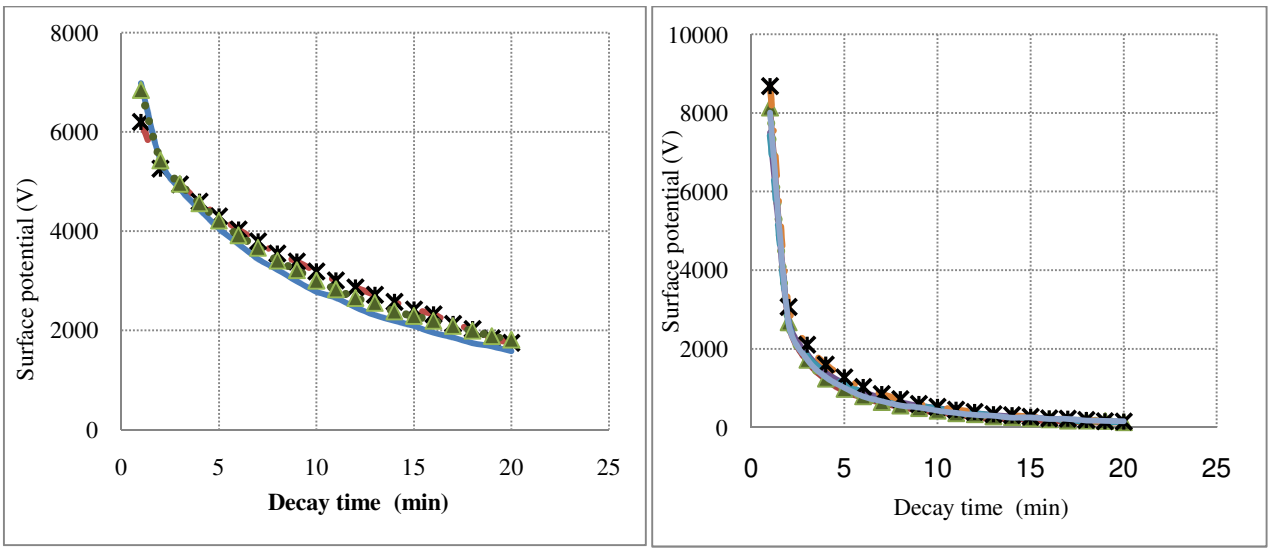

(a)

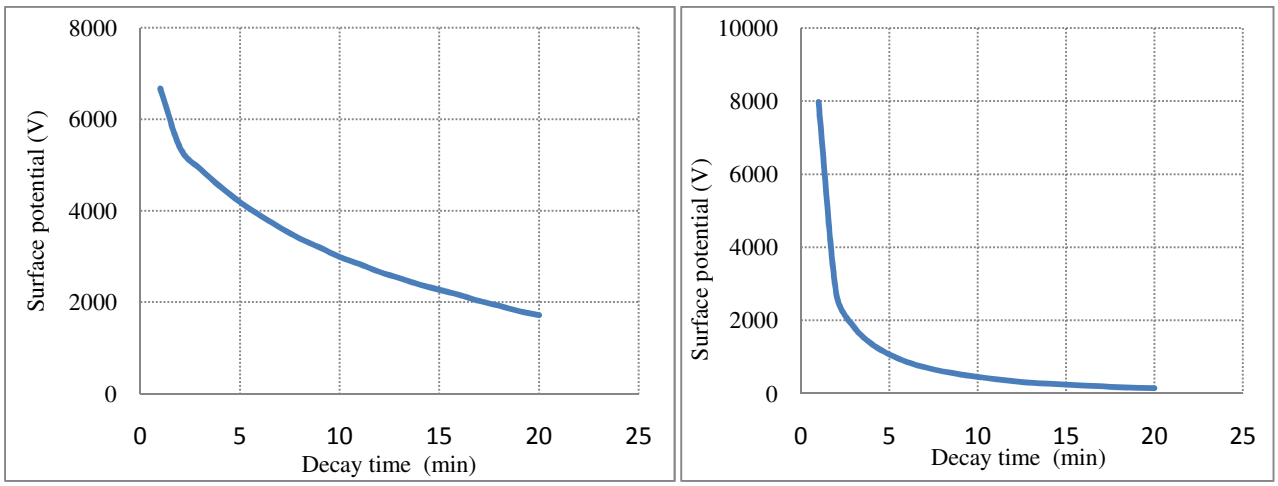

(b)

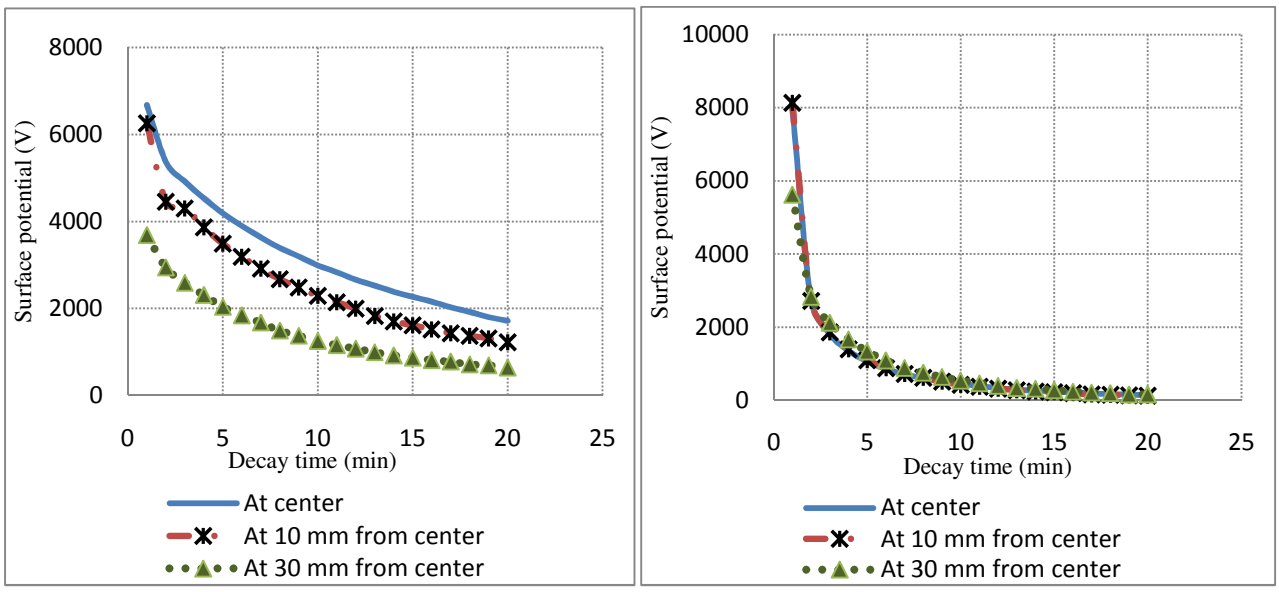

(c)

Figure 3.15. Decay of the surface potential for positively charged SIR and RTV-SIR samples. Charging voltage +20 kV, left column for SIR, right for RTV-SIR. The measured data at the center (a), averaged characteristics (b), results for different locations on the sample surface.

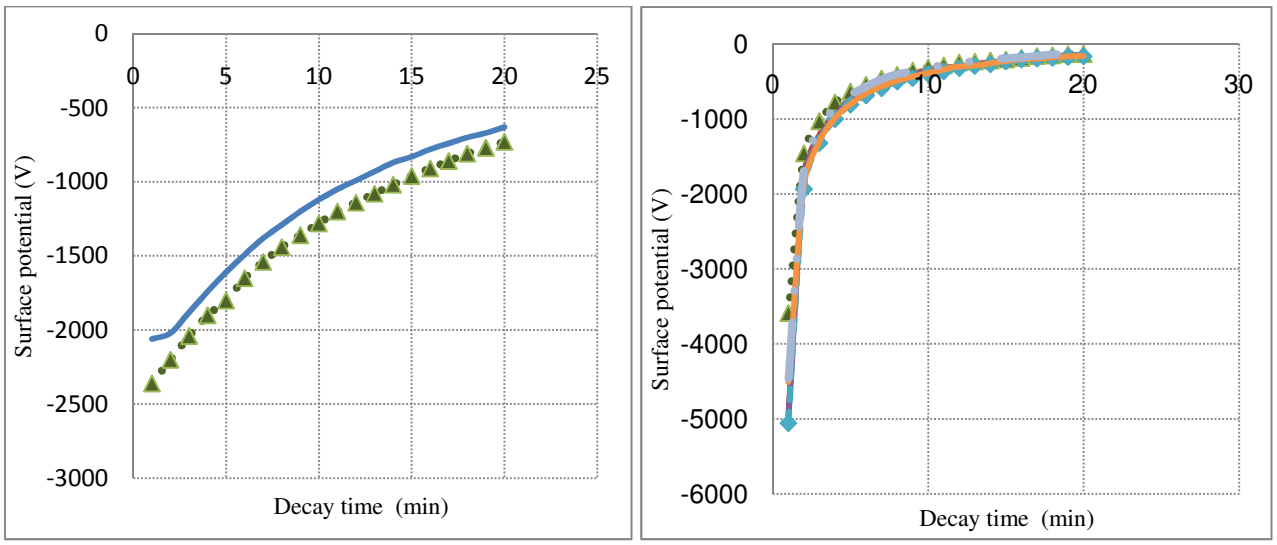

(a)

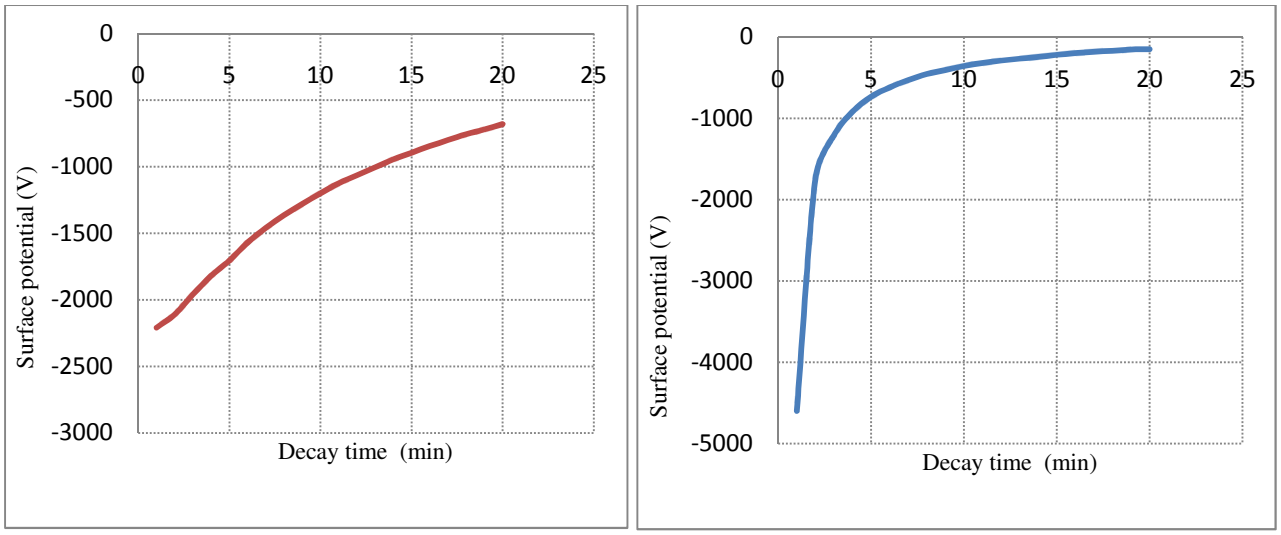

(b)

Figure 3.16. Decay of the surface potential for negatively charged SIR and RTV-SIR samples. Charging voltage -15 kV, left column for SIR, right for RTV-SIR. The measured data at the center (a), averaged decay characteristics (b).

CHAPTER 4

4. EXPERIMENT ON FLASHOVER VOLTAGE CHARACTERSTICS

4.1. Experimental set-up and procedures

Initially, the FO voltage tests were conducted in air medium between two electrodes with Rogowiski profile. Afterwards, samples of materials were inserted between the electrodes and the tests with clean surfaces were performed following the steps outlined in the procedure-I above. The experimental set-up for the test in air is illustrated in figure 4.1. In this arrangement, the air gap distance between the electrodes was made to be the same as the height of the utilized polymeric samples (i.e. 104mm). These experiments were done in order to obtain reference data for comparisons of the FOV characteristics in the gas medium alone and when the dielectric samples were inserted. Finally, the experimental set-ups outlined in Figures 3.2 and 3.3 were used in the rest of the investigation.

The procedures governing the FOV tests on LI pre-charged samples were explained in section Procedure-I above. For the dc-corona charged samples, the procedures for determining the flashover voltage characteristics were somewhat different. First, dc-charging voltage was applied to the corona belt for 2 minutes. After that, the charging belt was quickly removed and positive impulse voltage U_i was applied just after 1 and 3 minutes for RTV-SIR and SIR material samples, respectively. If a flashover along the insulator surface occurred, the next impulse voltage amplitude was decreased by 3 kV, otherwise the impulse voltage amplitude was increased. To avoid the surface charges accumulated on the insulator surface due to previous voltage application, the insulator samples were discharged (cleaned with alcohol). This step was crucial because the deposited potential might have impact on following impulse, no matter if a flashover occurred or not. The process was repeated until at least six FO events were recorded. After that, the averaged flashover voltage was calculated.

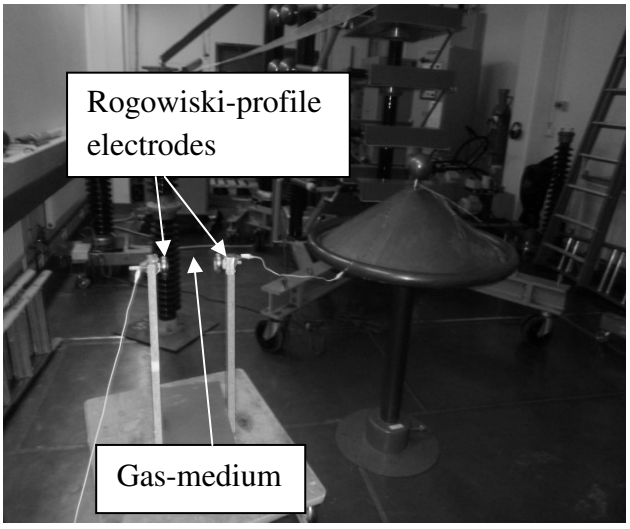

Figure 4.1. Electrode arrangement for FOV test between two metal electrodes

The flashover voltages were also investigated when the surface was charged to the opposite polarity as compared to the applied impulse polarity. In this case, the initial voltage level of the applied

impulse of opposite polarity was approximately $0.7U_{av}$ as previously stated, and if the sample didn't flashover, the sample surface was charged again and another impulse of higher magnitude (usually 3kV) was applied. This procedure was repeated until six or more flashover voltages for a given voltage were recorded.

All the FO voltages were corrected to standard air density. The tests were performed in normal laboratory air, the humidity was practically constant during the tests and the time between consecutive impulses was roughly constant. During the flashover voltage tests, the increment or decrement of the applied voltage level was approximately 3kV.

4.2. Test results and discussion

The results of the measurements of $U_{50\%}$ flashover voltages in air gap of 104 mm between the metallic electrodes are shown in Figure 4.2. As one may observe, the polarity effect is significant due to the relatively long distance between the electrodes as compared to their diameter that led to a non-uniform field distribution in the gap despite of smooth profiles of electrodes surfaces. Insertion of a material sample between the electrodes caused a reduction of the negative flashover voltages. In contrast to that, the FOVs for positive impulses showed nearly the same magnitudes independently on presence of a sample.

The measured flashover voltages of the samples pre-stressed by applying LI of the same polarity are shown in Figures 4.3-4.4. As one can see, the surface potential induced during charging is extremely small and its effect on FOVs is negligible. However in case of opposite polarities of the stressing and test impulses, the influence of the material can be recognized, Figure 4.5. In this case, pre-charging lead to some increase of flashover voltages as compared to the reference magnitudes in Figure 4.2.

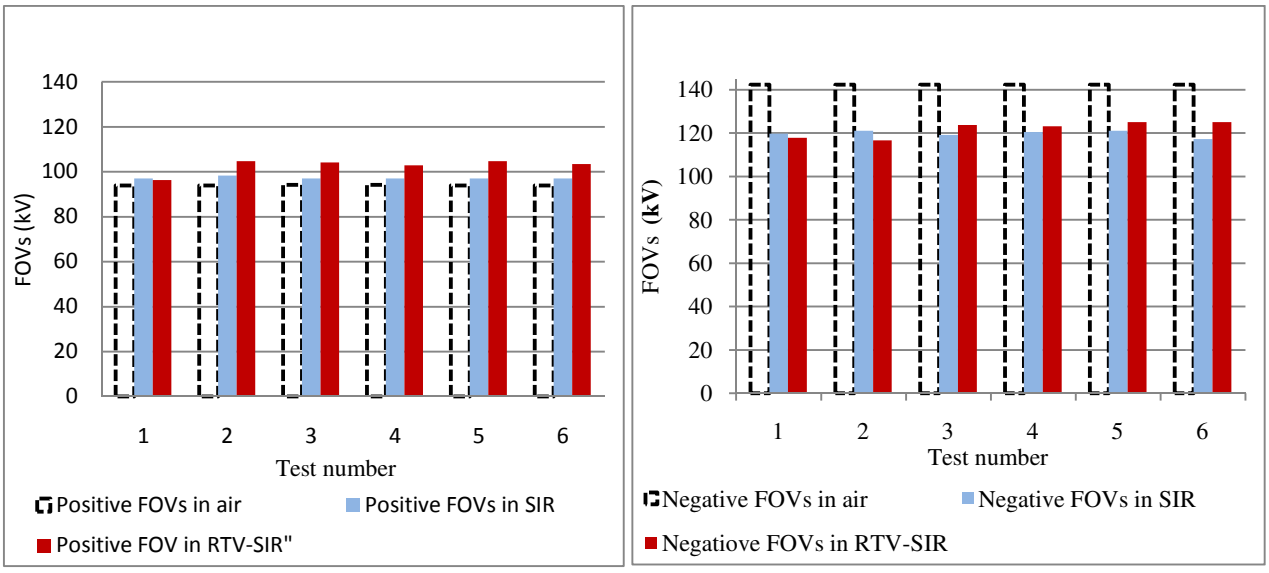

Figure.4.2.Positive (a) and negative (b) flashover voltages in air and in presence of SIR and RTV-SIR samples

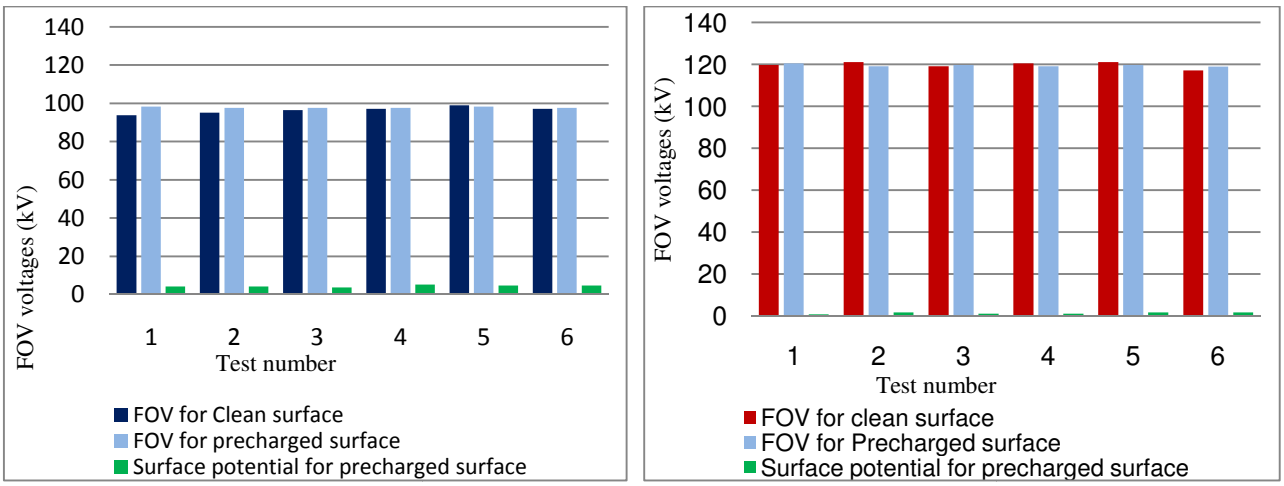

(a) (b)

Figure 4.3 Positive (a) and negative (b) flashover voltages for SIR samples

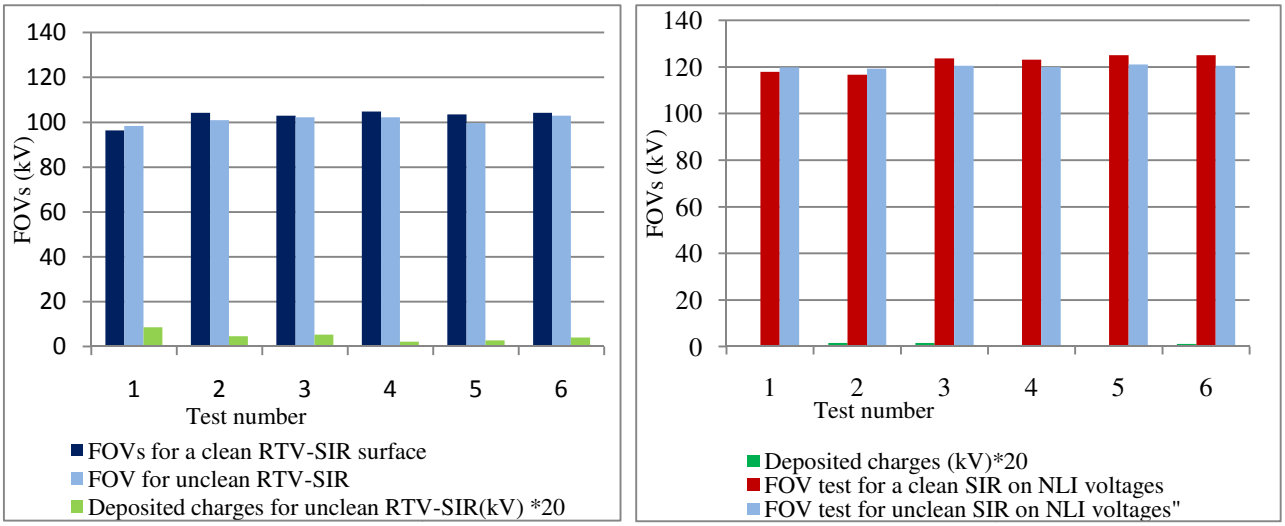

(a) (b)

Figure 4.4 Positive (a) and negative (b) flashover voltages for RTV-SIR samples

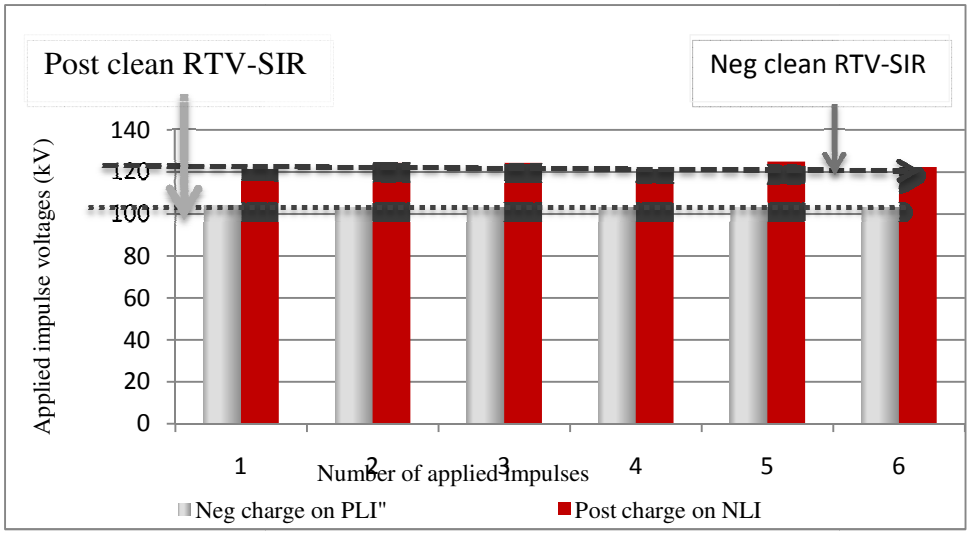

Figure 4.5 Flashover voltage measurements on pre-charged SIR samples of opposite polarities as the applied impulse voltages

In contrast to the considered results, corona charging of the insulators led to much more pronounced differences in the flashover characteristics. The results of all the performed experiments are summarized in Tables 5.1 and 5.2 for SIR and RTV-SIR materials, respectively. As one can see, an enhancement of the flashover performance in the presence of the deposited surface charges by corona takes place irrespectively of the polarity of the applied impulse voltages. However, the increase of FOVs is different for different materials and at different charging polarities. The former might be due to the difference in the surface charge behavior discussed in section 3 above while the latter may be related to variations of discharge conditions during charging. Thus, the corona starts earlier at negative polarity and the reference charging current of 0.1mA have been obtained at -15kV while for positive corona the current was reached at +20 kV. In addition to that, the surface potential profiles

Table 5.1 Impulse FOV measurement on SIR samples

Charging Source	Charges	Positive impulse voltage (kV)	Negative impulse voltage (kV)
	Air ($U_{50\%}$)	**92**	**139**
	No charges	**94**	**118**
Charged by Lightning impulse	**Positive Charges**	**94**	**118**
	Negative charges	**99**	**116**
Charged by corona-discharge	**Positive charges**	**96**	**125**
	Negative charges	**88**	**124**

Table 5.2 Impulse FOV measurements on RTV-SIR samples

Charging Source	Charges	Positive impulse voltage (kV)	Negative impulse voltage (kV)
	Air (U50%)	**92**	**139**
	No charges	**98**	**117**
Charged by Lightning Impulse	**Positive Charges**	**97**	**117**
	Negative charges	**99**	**118**
Charged from corona source	**Positive charges**	**110**	**152**
	Negative charges	**106**	**137**

obtained for the negative dc-corona charging were more symmetrical and repetitive for -15kV charging voltage level. Hence, the magnitudes of the deposited surface charges can be correlated with the flashover voltage characteristics.

The flashover voltages due to corona charging were found to be higher for the RTV-SIR material than for the SIR sample. These can be also related to materials properties (resistivity and permittivity). In particular, RTV-SIR is more resistive material than SIR and this property may provide different distribution of the electric field when the test voltage is applied as compared to the case of SIR. This issue can be elucidated further by means of computer simulations.

CHAPTER 5

5. CONCLUSION AND FUTURE WORK

5.1 Conclusion

Surface charging by pre-stressing LI impulses and by dc corona was experimentally investigated on samples of SIR and RTV-SIR materials and the effect of the deposited charges on the flashover characteristics was studied.

Surface potential dynamics, its distributions and decay were investigated experimentally. It was observed that the spatial and temporal variations of the surface potential were almost similar for each material samples in both polarities. During impulse pre-stressing, the magnitudes of the surface potentials were observed to be increasing or decreasing depending on the applied impulse voltage while the polarity of the applied impulse voltage didn't show any significant effect on the measured surface potential values. Measurements on corona charges samples showed that the magnitudes of the surface potential on RTV-SIR material were higher and the potential decay was faster than those measured on the SIR sample. This might be related to the differences in the material compositions which can result in different properties.

The flashover voltages were found to be affected by presence of insulating material between electrodes. The insertion of a cylindrical sample between the electrodes led to a reduction of the measured FOVs in the negative impulse tests as compared to those for air medium, but no significant differences were observed at positive polarity.

During pre-stressing with LI voltages, the polarity of the deposited surface charges on the insulators surfaces was the same as the polarity of the applied impulse. The FOVs magnitudes for the negative impulse were higher than that for positive ones for clean surfaces of the samples. An enhancement of the impulse performance of SIR insulator at negative polarity was found when the insulator was charged by negative dc corona. The FOVs on RTV-SIR sample were slightly higher than that on SIR sample. In general, one may conclude that flashover characteristics of the materials samples were affected by the presence of deposited surface charges, despite the polarities of the deposited charges.

5.2. Future work

The thesis work presented here focused mainly on the effect of surface charges deposited by dc-corona and pre-applied impulse voltages on the flashover characteristics. The materials used here were only RTV-SIR and SIR. To compare the effect of the material composition on the presented results, another more material samples are suggested to be tested and the standard properties of the materials is of prime requisite to be known. Hence standard material types are recommended to carry out the experimental tests.

A system for simultaneous control of experimental parameters such as pressure, ambient air and humidity can be developed. The experimental set up for the corona charging of the samples should be modified in a way that the charging belt supports shouldn't touch the material samples. This

would allow for avoiding additional charge deposition during the contact between the samples and the corona charging belt supports.

The experiment done for the spatial and temporal variations of surface potential and potential decay measurements after charging should be done as many times as possible to get more properties of the surface charges effect on the flashover performances. To avoid some loss of surface charges during the measurement period, the measurement time (scanning time) should as short as possible.

A general mathematical model of the observed effects based on physical properties of the studied materials can be very beneficial for a deeper analysis.

This is a task well began. While some progress has already been made, much still remains to be done. I hope that this work will provide a significant point of reference for future endeavors.

REFERENCES

[1] G.Asplund, "*Sustainable energy systems with HVDC transmission*", IEEE Power Eng. Soc. general meeting, Vol.2, pp.2299-2303, 2004.

[2] Www.energy consumption forecast/International Energy Outlook 2010 – Highlights.

[3] H. Sjöstedt, "*Electric charges on insulator surfaces and their influence on insulator performance*", Doctoral thesis at CHT, 2008.

[4] S. Kumara, "*Electrical charges on polymeric insulator surfaces and their impact on flashover performance*", Doctoral thesis at CHT, 2009.

[5] P.Moliniet, M. Goldmant and J.Gatellet*," Surface potential decay on corona-charged epoxy samples due to polarization processes*", J. Physic. D. Appl. Physic, Vol. 28, No.8, pp.1601-1610,1995 .

[6] G.M.Sessler,"*Electrets Volume 1,third edition*", Laplacianpress, 1998.

[7] T.Jing, P.H.F.Morshuis and F.H.Kreuger, Delft,The Netherlands, "*Mechanisms of surface charge accumulation in SF6*", Arch. Elect, No.77, pp.151-155, 1994.

[8] H. Fujinami, T. Takuma, M. Yashima and T. Kawamoto, "M*echanism and Effect of dc charge accumulation on SF6 gas insulated spacers"*, IEEE Trans.P.Delivery, Vol. 4,1989.

[9] F.messerer, M.Finkel, W.boeck, *"Surface charge accumulation on HVDC-GIS spacer",* IEEE Inter. Symp. Elect. Insul. Boston, MA USA,2002.

[10] F.Wang, Y.Qiu, Zhang,X.Q.Qiu, E.kuffel,"*Insulator Surface Charge Accumulation under Impulse Voltage*" IEEE Trans.on Diel. and Elect. Insul, Vol. 11, No. 5; October 2004.

[11] S.G.J.Ehnbergand, H.J.M.Blennow,"*Effects of surface charge accumulation on impulse flashover voltage on silicon rubber surface*", Proc.13th Int. Symp Delft, Netherlands, pp.242, August 2003.

[12] C.M.Cooke,"*Charging of insulator surfaces by ionization and transport in gases*", IEEE trans. on elect. insul,VOl.1, No.2, E1-17,April 1982.

[13] C.L.Wadhwa,"*High voltage engineering* ",Second edition,2007.

[14] Yuri P.Raizer*," Gas discharge physics"* Second edition 1991.

[15] S. Place, Liondon*"Gas discharge physics",* 1996.

[16] M. Akyuz, "*Positive streamer discharge in air and along insulating surfaces: experiment and simulation",* Doctoral thesis at Uppsala University, 2002.

[17] S. Le. Roy, P. Segur, G. Teyssedre and C. Laurent," *Description of bipolar charge transport in polyethylene using a fluid model with a constant mobility", J.Phys.D,* Vol 37, pp. 298-305, 2004.

[18] J. A. Giacometti, S. Fedosov and M. M. Costa, "*Corona charging of polymers: Recent Advances on constant current Charging*", Brazilian J.Phys, Vol. 29, No. 2, 1999.

[19] Al-Bawy, Prof.O. Farish,"*Charge deposition on an insulating spacer under impulse voltage*", IEEE proc.A, Vol.138, No-3, May 1991.

[20] EA. Baum, T. J. Lewis and R. Toomer, "*Decay of electrical charge on polyethylene films*", J. Phys. D: Appl. Phys, Vol. 10, 1977.

[21] G. Chen*, "A new model for surface potential decay of corona-charged polymers", J.Phy.D,* Vol 43, 2010.

[22] G.Chen, Z. Xu and LW. *Zhang, "Measurement of surface potential decay of corona-charged polymer films using the pulsed electroacoustic method",* Meas. Sci. Technol, Vol.18,pp 1453–1458 2007.

[23] Z. Xu, L. Zhang and G. Chen,"*Decay of electric charge on corona charged polyethylene",* J. Phys. D: Appl. Phys. 40 pp.7085–7089,2007.

[24] T.J.Sonnonanstine and M.M. Perlm, *"Surface potential decay in insulators with field dependent mobility and injection efficiency"* J. app,Phys,Vol.46, No.9,1975.

[25] J. Kindersberger and C.Lederle,*"Surface charge decay on insulators in air and sulfurhexafluorid–Part I: Simulation",* IEEE Trans.Diel and Elect. Insul, Vol. 15, No. 4; 2008.

[26] J. Kindersberger and C. Lederle,*"Surface charge decay on insulators in air and sulfurhexafluorid–Part II: Measurements",* IEEE Trans. Diel and Elect. Insul, Vol. 15, No. 4, 2008.

[27] M.Ieda, G.Saws and U.Shinihawa, "*A decay process of surface electric charges across polyethylene films", J.app.phys*.,Vol 6, pp.739-794,1967.

[28] M.Ied*a, "Electrical conduction and carrier traps in polymeric materials",* IEEE trans.Elect.Insul, Vol.19, No.3 pp.16-178,1984.

[29] P.Llovera and P.Molinie, "*New methodology for surface potential decay measurements: application to study charge injection dynamics on polypropylene films*", IEEE Trans. Diel and Elect. Insul, Vol. 11, No. 6, December 2004.

[30] P.Molinie, "*Charge injection in corona-charged polymeric films: potential decay and current measurements",*J.Electrostatics,Vol 45, pp.265-273,1998.

[31] J.M. Alison and R. M. Hill,"*A model for bipolar charge transport, trapping and recombination in degassed crosslinked polyethene*", J.phys.D, Vol.27,pp.1291-1299,1994.

[32] P. Molinie, M. Goldman and J. Gatellet, " *Surface potential decay on corona-charged epoxy samples due to polarization processes",* J. Phys.D. Appl. Phys, Vol.28, pp 1601-1610, 1995.

[33] A. Neves, Helvio, J.A.Martins, "*Surface charging and charge decay in solid dielectrics",* IEEE Inter.Symp, Montereal, 1996.

[34] A.Crisci, B.Gosse, J-P.Gosse and V.Ollier-Dureault, "*Surface potential decay due to surface conduction*", Eur.Phys.J.AP, VOl.4, pp.107-116,19998.

[35] M.S.A.A. Hammam, S. Ochiai and Clayton Burns, "*Effect on 50% flashover voltage due to accumulated charges on the surface of polymer insulators"*, Prop and Appl.Diel. Materials, 1991.

[36] J. Blennow, T. Sörqvist, "*Effect of surface charge on flashover voltage of polymer materials*", Proc.19th Nordic Insul. Symp, NORD-IS 05,Trondheim, pp.262-265 June 2005.

[37] R. Montaño, H. Sjöstedt, Y. Serdyuk, S.M. Gubanski, " *Effect of Surface Charges on the Flashover Voltage Characteristics of Polymeric materials: Comparison between Theory and Practice*", Ann. Rep. Conf.Elect. Insul and Diel.Phenomena,2007.

[38] Xie Jun and I D Chalmers, "*The influence of surface charge upon flash-over of particle-contaminated insulators in SF6 under impulse-voltage conditions",* J. Phys. D: Appl. Phys.Vol.30, pp.1055–1063,1997.

[39] H. Sjöstedt, S.M. Gubanski and Y. Serdyuk, "*Charging Characteristics of EPDM and silicone rubbers deduced from surface potential measurements*", IEEE Trans. Diel and Elect. Insul, Vol. 16, No. 3, 2009.

[40] M. Darveniza, T.K. Saha, M. A. Leijon, S. Wright, " *Effect of deposited charge on impulse test techniques for polymer insulators*", Cigre,2001.

[41] H.J.Wintle, " *Surface-charge decay in insulators with none constant mobility and with deep trapping "*, J.Appl. Phys, vol.43,No.7, pp. 2927-2930,1972.

[42] D. K. Das-Gupta, " *Decay of electrical charges on organic synthetic polymer surfaces",* IEEE Trans.Elect. Insul, Vol. 25, No. 3, June 1990.

[43] T. G.Gustavsson, " *Silicon rubber insulators- impact of material formulation in costal environment"*, Doctorial thesis,CTH Sweden, 2003.

[44] S. Wallström "*Biofilms on silicon rubber material for outdoor high voltage insulation*", Doctorial thesis, KTH Sweden,2005.

[45] E. A. Cherney and R.s. Gorur, "*RTV silicone rubber coatings for outdoor insulators"*, IEEE Trans. Diel. and Elect. Insul, Vol. 6, No. 5, 1999.

[46] F.Wang, Y.Qiu,q, Zhang,X.Q.Qiu, E.kuffel, "*Initial conditions of surface charge accumulation under impulse voltage",*Ann. Conf. Prep, 2002.

[47] M. Sjöberg, "*Charge accumulation in hybrid high voltage insulation*", Doctoral thesis at CHT Sweden, 2003.

[48] F.Messer, M.Finkel, W.Boeck*, "Surface charge accumulation on HVDC-GIS-Spacer",* IEEE Int. Symp, Boston, 2002.

[49] A.Winter and J.kindersberger*, "surface charge accumulation on insulating plateds in SF6 and the effect on DC and AC breakdown voltage of electrode arrangements",*Inst.High Volt Eng and Electr. P. Trans, Germany.

[50] E. Kuffel, W.S.Zaengl,J.kuffel,"*High voltage engineering fundamentals*", Second edition,2000.

[51] T.Blytheand, D.Bloor, "*Electrical properties of polymers",* Cambrdge Univ.Pres, 2005.

[52] I.P.Batra, K.Keijli Kanazawa, B.H.schechtman and H.Seki, "*Charge-carrier dynamics following pulsed photoinjection",* Jornal of Applied Physics, Vol.42, pp.1124-1130, 1971.

APPENDIXES

Appendix [A]: Applied NLI voltage on a clean RTV-SIR surface

	Applied impulse voltage (kV)				Surface Pot before FOV (kV)				Flashover voltage(F		Surface pot just after FOV (kV)			
	Negative Polarity		Positive polarity		Negative Polarity		Positive polarity		Grd plt FO yes = 1	Flt plt FOV yes = 1	Negative Polarity		Positive polarity	
Number o	Grd plt	Flt plt	Grd plt	Flt plt	Grd plt	Flt plt	Grd plt	Flt plt	No = 0	No = 0	Grd plt	Flt plt	Grd plt	Flt plt
1	97,68	97,68			0,42	0,16	3,2		0	0				
2	100,9	98,33			0,35	0,19	3,8		0	0				
3	101,6	97,68			0,28	0,2	4		0	0				
4	103,5	101,6			0,33	0,23	4,6		0	0				
5	102,9	102,2			0,33	0,25	5		0	0				
6	105,5	106,1			0,3	0,3	6		0	0				
7	105,5	105,5			0,48	0,39	7,8		0	0				
8	106,1	106,8			0,28	0,44	8,8		0	0				
9	107,4	104,8			0,28	0,53	10,6		0	0				
10	108,7	110			0,3	0,43	8,6		0	0				
11	111,4	110			0,27	0,4	8		0	0				
12	112	111,4			0,43	0,29	5,8		0	0				
13	112,7	109,4			0,5	0,35	7		0	0				
14	114,6	113,3			0,58	0,42	8,4		0	0				
15	117,9	117,9			0,62		0		0	1		0,02		
16	117,9	115,9			0,61	0,47	9,4		0	0				
17	117,9	116,6			0,6		0		0	1		0,08		
18	117,9	115,9			0,26	0,63	12,6		0	0				
19	120,5	115,9			0,64	0,42	8,4		0	0				
20	119,8	117,2			0,74	0,39	7,8		0	0				
21	125,7	113,3				0,45	9		1	0	0,03			
22	123,7	116,6			0,24		0		0	1		0,08		
23	122,4	119,5			0,58	0,38	7,6		0	0				
24	124,4	120,5			0,88	0,41	8,2		0	0				
25	125,1	123,7			0,74		0		0	1		0,02		
26	126,3	119,8			0,68	0,4	8		0	0				
27	128,9	123,1					0		1	1	0,05	0,03		
28	125	125			0,46	0,06	1,2		0	1		0,06		
29	125	125			0,61	0,04	0,8		0	1		0,04		
30	128,3				0,02		0		1		0,02			
31	127				0,03		0		1		0,03			
						Surface Potential pre flashover voltage = 121 kV								
						Surface Potential pre flashover voltage = 121 kV								

Appendix [B]: Applied NLI voltage on a clean SIR surface

	Applied impulse voltage (kV)				Surface Potential before FOV (kV)				ashover voltage(FO		Surface potential just after FOV (k			
	Negative Polarity		Positive polarity		Negative Polarit		Positive polarity		Grd plt FO yes = 1	Flt plt FO yes = 1	Negative Polarity		Positive polarity	
Number	Grd plt	Flt plt	Grd plt	Flt plt	Grd plt	Flt plt	Grd plt	Flt plt	No = 0	No = 0	Grd plt	Flt plt	Grd plt	Flt plt
1	109,5	106,1			1,4	0,47	9,4		0	0				
2	109,4	107,44			1,58	0,67	13,4		0	0				
3	107,4	107,4			1,41	1,65	33		0	0				
4	112	108,1			1,45	0,8	16		0	0				
5	113,3	109,4			1,6	0,78	15,6		0	0				
6	113,3	110,7			1,63	1,01	20,2		0	0				
7	113,3	111,4			1,66	1,14	22,8		0	0				
8	114	111,4			1,54	1,41	28,2		0	0				
9	115,9	116,6			1,45	1,54	30,8		0	0				
10	114,6	112,7			1,5	1,51	30,2		0	0				
11	116,6	116,6			1,54	1,64	32,8		0	0				
12	112,7	118,5			1,62	1,67	33,4		0	0				
13	117,9	119,8			1,8	1,69	33,8		0	0				
14	118,5	119,2			2,03	1,73	34,6		0	0				
15	119,8	119,8			2,24		0		0	1		0,2		
16	118,5	120,5			2,29	1,31	26,2		0	0				
17	119,8	117,9			2,24	1,45	29		0	0				
18	121,1	121,1					0		1	1	0,28	0,09		
19	120,8	119,2			1,2		0		0	1		0,12		
20	121,1	117,2			1,78	1,28	25,6		0	0				
21	121,1	120,5			1,93		0		0	1		0,11		
23	123,1	121,1			1,78		0		0	1		0,12		
24	120,5	119,2			1,9	1,31	26,2		0	0				
25	124,4	117,2					0		1	1	0,3	0,11		

Average Flashover voltage with grounded plate=120,6 Kv Surface Potential pre flashover voltage = 0 Kv

Average Flashover voltage with floating plate=119.8Kv Surface Potential pre flashover voltage = 0 Kv

Appendix [C]: Applied NLI voltage on a positively pre-charged SIR surface

	Impulse charging voltage (kV)				Applied Impulse voltage (kV)				Surface Pot before FOV (kV)				Flashover voltage (F		Surface pot just after FOV (kV)			
	Negative Polarity		Positive polarity		Negative Polarity		Positive polarity		Negative Polarity		Positive polarity		Grd plt FO yes = 1	Flt plt FOV yes = 1	Negative Polarity		Positive polarity	
Number o	Grd plt	Flt plt	Grd plt	Flt plt	Grd plt	Flt plt	Grd plt	Flt plt	Grd plt	Flt plt	Grd plt	Flt plt	No = 0	No = 0	Grd plt	Flt plt	Grd plt	Flt plt
1			82,7															
2			83,35															
3			82,7															0,12
4	42,5	45			117,2	121,8			0,25	0,75	0,3	0,65	0	0				
5			76,19															
6			70,98															
7			64,47															
8	43	46			118,7	123,7			0,27		0,45	0,36	0	1		0,07		
9			72,28															
10			74,88															
11			76,19															
12	43,5	45			119,8	117,9			0,39	0,64	0,39	0,52	0	0				
13			82,7															
14			83,35															
15			82,7															
16	44	44	45,5		121,1	119,1				0,19	0,64	0,3	1	0	0,73			
17			82,7															
18			82,7															
19			82,7															
20	44,5				119,8				0,2		0,32	0,63	0	0		0,13		
21			82,05															
22			83,05															
23			83,35															
24	45				124,4						0,3		1		0,02			
25			83,35															
26			83,35															
27			83,35															
28	44,5				124,4						0,32		1		0,03			
29			82,7															
30			83,35															
31			83,35															
32	44				121,1						0,3		1		0,03			
33			76,19															
34			77,49															
35			83,35															
36	43,5				120,5				0,24		0,35		0					
37			83,35															
38			83,35															
39			83,35															
40	43,8				125						0,35		1		0,05			
41			83,35															
42			84															
43			84															
44	43,5				121,1				0,18		0,33		0					
45			84															
46			84															
47			84															
48	43,8				122,4						0,35		1		0,06			

Average Flashover voltage with grounded plate = -123 Kv

Appendix [D]: Applied NLI voltage on a pre-charged RTV-SIR surface

	Applied impulse voltage (kV)				Surface Pot before FOV (kV)				Flashover voltage(FO		Surface pot just after FOV (kV)			
	Negative Polarity		Positive polarity		Negative Polarity		Positive polarity		Grd plt FO yes =1	Flt plt FOV yes = 1	Negative Polarity		Positive polarity	
Number o	Grd plt	Flt plt	Grd plt	Flt plt	Grd plt	Flt plt	Grd plt	Flt plt	No = 0	No = 0	Grd plt	Flt plt	Grd plt	Flt plt
1	105,5	106,1			0,26	0,22			0	0				
2	106,8	107,4			0,3	0,36			0	0				
3	107,4	107,4			0,29	0,39			0	0				
4	108,7	108,1			0,54	0,38			0	0				
5	108,7	108,7			0,38	0,38			0	0				
6	109,4	109,4			0,51	0,4			0	0				
7	110,7	99,3			0,48	0,26			0	0				
8	112	99,63			0,45	0,26			0	0				
9	112,7	115,9			0,52	0,46			0	0				
10	113,3	116,6			0,45	0,46			0	0				
11	115,3	115,3			0,4	0,4			0	0				
12	115,9	115,3			0,48	0,51			0	0				
13	116,6	118,5			0,6	0,3			0	0				
14	117,2	118,5			0,64	0,43			0	0				
15	116,6	118,5			0,63	0,43			0	0				
16	119,2	119,8							1	1	0,01	0,03		
17	117,9	119,2			0,5				0	1		0,02		
18	118,5	117,9			0,57	0,29			0	0				
19	118,5	119,2			0,6	0,41			0	0				
20	119,8	119,8			0,56	0,46			0	0				
21	119,8	120,5				0,39			1	0	0,01			
22	119,2	120,5			0,46				0	1		0,02		
23	120,5	119,2			0,48	0,3			0	0				
24	122,4	121,1				0,3			0	0	0,08			
25	119,8	122,4			0,5	0,36			0	0				
26	120,5	123,7			0,6				0	1		0,04		
27	122,4	122,4			0,6				1	1		0,03		
28	123,7	119,8				0,21			0	0	0,03			
29	120,5	121,1			0,4				0	1		0,02		
30	121,8	120,5							1	1	0,01	0,03		
						Surface Potential pre flashover voltage = 120,75 kV								
						Surface Potential pre flashover voltage = 121 kV								

Appendix [E]: Applied NLI voltage on a pre-charged SIR surface

	Applied impulse voltage (kV)				Surface Potential before FOV (kV)				ashover voltage (FOV		Surface potential just after FOV (kV)			
									Grd plt FO	Flt plt FOV				
	Negative Polarity		Positive polarity		Negative Polarity		Positive polarity		yes = 1	yes = 1	Negative Polarity		Positive polarity	
Number o	Grd plt	Flt plt	Grd plt	Flt plt	Grd plt	Flt plt	Grd plt	Flt plt	No = 0	No = 0	Grd plt	Flt plt	Grd plt	Flt plt
1	98,33	112		5,2	0,26	0,08			0	0				
2	101,6	112,7		8,6	0,43	0,13			0	0				
3	102,9	113,3		9,2	0,46	0,18			0	0				
4	102,9	114,6		11,8	0,59	0,24			0	0				
5	103,5	115,9		12	0,6	0,24			0	0				
6	104,2	116,6		10,8	0,54	0,25			0	0				
7	106,1	116,6		12,4	0,62	0,26			0	0				
8	107,4	117,9		14	0,7	0,27			0	0				
9	108,1	118,5		13,4	0,67	0,29			0	0				
10	109,4	119,8		14,4	0,72	0,32			0	0				
11	110	120,5		14,6	0,73	0,32			0	0				
12	113,3	121,1		13,2	0,66				0	1		0,04		
13	112	120,5		12,6	0,63	0,29			0	0				
14	115,3	121,1		15,8	0,79				0	1		0,03		
15	117,2	119,2		14,6	0,73	0,2			0	0				
16	116,6	120,5		14,6	0,73				0	1		0,02		
17	120,5	118,5		0		0,2			1	0	0,08			
18	120,5	120,5		7,8	0,39				0	1		0,02		
19	119,8	119,2		7,6	0,38	0,19			0	0				
20	120,5			8,6	0,43				0					
21	119,2			0					1		0,18			
22	119,2			8,6	0,43				0					
23	120,5			10,2	0,51				0					
24	119,8			0					1		0,11			
25	118,5			9	0,45				0					
26	120,5			0					1		0,11			
27	119,5			0					1		0,18			
28	119			0					1		0,18			
					Average flashover voltage with grounded plate = -120Kv									
					Average flashover voltage with floating plate = -119,5Kv									

Appendix [F]: Applied NLI voltage on air medium

	Applied impulse voltage (kV)				Surface Pot before FOV (kV)				Flashover voltage(F		Surface pot just after FOV (kV)			
	Negative Polarity		Positive polarity		Negative Polarity		Positive polarity		Grd plt FO yes = 1	Flt plt FOV yes = 1	Negative Polarity		Positive polarity	
Number o	Grd plt	Flt plt	Grd plt	Flt plt	Grd plt	Flt plt	Grd plt	Flt plt	No = 0	No = 0	Grd plt	Flt plt	Grd plt	Flt plt
1	40				-109,8				0					
2	40				-109,8				0					
3	40				-109,8				0					
4	40				-109,8				0					
5	43				-118,1				0					
6	43				-118,1				0					
7	43				-118,1				0					
8	43				-118,1				0					
9	45				-122,6				0					
10	45				-122,6				0					
11	45				-122,6				0					
12	45				-122,6				0					
13	47				-128,7				0					
14	47				-127,9				0					
15	47				-127,9				0					
16	47				-128,7				0					
17	50				-137				0					
18	50				-136,3				0					
19	50				-136,3				0					
20	50				-136,3				0					
21	51				-138,5				0					
22	51				-139,3				1					
23	51				-139,3				0					
24	51				-139,3				0					
25	51				-139,3				0					
26	51				-139,3				0					
27	51,5				-140,8				0					
28	51,5				-140				0					
29	51,5				-140,8				1					
30	51,5				-140				0					
31	51,5				-140				1					
32	51,5				-140,8				0					
33	51,5				-140				0					
34	51,5				-140,8				0					
35	51,5				-140,8				1					
36	51,5				-140				0					
37	51,5				-140,8				0					
38	51,5				-140,8				1					
39	52				-142,3				1					
40	52				-142,3				0					
41	52				-142,3				1					
42	52				-142,3				0					
43	52				-142,3				0					
44	52				-142,3				0					
45	52				-142,3				1					
46	52				-142,3				0					
47	52				-142,3				1					
48	52				-142,3				0					
49	52				-142,3				1					
50	52				-142,3				0					
51	53				-144,6				1					
52	53				-144,6				0					
53	53				-144,6				1					
54	53				-144,6				0					
55	53				-144,6				1					
56	53				-144,6				0					
57	54				-147,6				0					
58	54				-147,6				1					
59	54				-147,6				0					
60	54				-147,6				1					
61	54				-147,6				0					
62	54				-147,6				1					
63	54				-147,6				0					
64	54				-147,6				1					
65	54				-147,6				0					
66	54				-147,6				1					
67	54				-147,6				0					
68	54				-147,6				1					
69	55				-149,9				1					
70	55				-149,9				1					
71	55				-149,9				0					
72	55				-149,9				1					
73	55				-149,9				0					
74	55				-149,9				1					
75	55				-149,9				0					
76	55				-149,9				1					
77	55				-149,9				0					
78	55				-149,9				1					
79	55				-149,9				0					
80	55				-149,9				1					
						Average Surface flashover voltage = 142 kV								

Appendix [G]: Applied PLI voltage on a clean RTV-SIR surface

	Applied impulse voltage (kV)				Surface Potential before FOV (kV)				ashover voltage (FOV		Surface potential just after FOV (kV)			
	Negative Polarity		Positive polarity		Negative Polarity		Positive polarity		Grd plt FOV yes = 1	Flt plt FOV yes = 1	Negative Polarity		Positive polarity	
Number o	Grd plt	Flt plt	Grd plt	Flt plt	Grd plt	Flt plt	Grd plt	Flt plt	No = 0	No = 0	Grd plt	Flt plt	Grd plt	Flt plt
1			92,47	93,77		6	0,3	0,33	0	0				
2			94,42	90,51		6,6	0,33	0,3	0	0				
3			93,77	96,37		7,6	0,38	0,33	0	0				
4			95,72	96,37		7	0,35	0,29	0	0				
5			92,47	97,68		5,8	0,29	0,19	0	1				0,19
6			96,37	94,42		0		0,3	1	0			0,06	
7			97,02	96,37		5,6	0,28	0,29	0	0				
8			97,02	97,02		5,2	0,26	0,28	0	0				
9			97,02	96,37		5,6	0,28	0,3	0	0				
10			98,98	98,33		6	0,3	0,28	0	0				
11			98,33	99,63		5,8	0,29	0,29	0	0				
12			99,63	101,6		5,2	0,26		0	1				0,16
13			101,6	95,72		5,8	0,29	0,25	0	0				
14			103,5	101,6		4,6	0,23	0,32	0	0				
15			104,8	101,6		0		0,32	1	0			0,04	
16			104,2	103,5		0			1	1			0,06	0,11
17			102,9	103,5		0		0,36	1	0			0,04	
18			93,12	103,5		4,4	0,22		0	1				0,05
189			104,8	102,9		0		0,29	1	0			0,06	
20			103,5	103,5		0			1	1			0,05	0,06
21			102,9			5,2	0,26		0					
22			103,5			5	0,25		0					
23			104,2			0			1				0,1	

FOV for positive impulse test on a clean surface gd plt =103kV

FOV for positive impulse test on a clean surface flt plt =103kV

Appendix [H]: Applied PLI voltage on a clean SIR surface

	Applied impulse voltage (kV)				Surface Potential before FOV (kV)				Flashover voltage (F		Surface potential just after FOV (kV)			
	Negative Polarity		Positive polarity		Negative Polarity		Positive polarity		Grd plt FO yes = 1	Flt plt FOV yes = 1	Negative Polarity		Positive polarity	
Number o	Grd plt	Flt plt	Grd plt	Flt plt	Grd plt	Flt plt	Grd plt	Flt plt	No = 0	No = 0	Grd plt	Flt plt	Grd plt	Flt plt
1			81,4	64,47			0,46	0,26	0	0	5,2			
2			82,05	65,12			0,43	0,16	0	0	3,2			
3			85,3	65,77			0,45	0,65	0	0	13			
4			84	65,12			0,35	0,25	0	0	5			
5			84,65	65,12			0,44	0,56	0	0	11,2			
6			87,26	65,12			0,51	0,38	0	0	7,6			
7			88,56	84			0,85	0,43	0	0	8,6			
8			89,21	87,91			0,73	0,46	0	0	9,2			
9			91,16	90,51			0,8	0,62	0	0	12,4			
10			91,82	90,51			0,74	0,78	0	0	15,6			
11			93,77	95,72			0,73	0,65	0	0	13			
12			93,77	97,02			0,8		0	1	0			0,34
13			96,37	95,72				0,74	1	0	14,8		0,34	
14			95,07	98,33			0,68		0	1	0			0,28
15			97,68	95,07				0,66	1	0	13,2		0,23	
16			96,37	97,02			0,73		0	1	0			0,34
17			97,02	97,02			0,76		0	1	0			0,23
18			98,98	97,02					1	1	0		0,3	0,23
19			97,02	97,02					0	1	0			0,28
					FOV for positive impulse test on a clean surface gd plt = 97kV									
					FOV for positive impulse test on a clean surface flt plt = 97kV									

Appendix [I]: Applied PLI voltage on a negatively pre-charged SIR surface

	Impulse charging voltage (kV)				Applied impulse voltage (KV)				Surface Potl before FOV (kV)				Flashover voltage (F		Surface pot just after FOV (kV)			
	Negative Polarity		Positive polarity		Negative Polarity		Positive polarity		Negative Polarity		Positive polarity		pre-charg yes = 1	Flt plt FO\ yes = 1	Negative Polarity		Positive polarity	
Number o	Grd plt	Flt plt	Grd plt	Flt plt	Grd plt	Flt plt	Grd plt	Flt plt	Grd plt	Flt plt	Grd plt	Flt plt	No = 0	No = 0	Grd plt	Flt plt	Grd plt	Flt plt
1	108,7	110																
2	108,7	112																
3	108,7	111,4																
4							104,2	97,02	0,3	0,92	0,5	0,42	0	1				0,12
5	106,8	110,7																
6	108,7	111,4																
7	108,7	110,7																
8							104,2	97,02	0,6	1,23		0,3	1	0			0,25	
9	107,4	110,7																
10	108,1	110																
11	106,8	111,4																
12							101,6	97,02	0,35	0,6	0,5	0,46	0	0				
13	107,4	109,4																
14	107,4	110																
15	107,4	110																
16							101,6	97,68	0,35	0,35	0,6	0,25	0	0				
17	107,4	109,4																
18	107,4	109,4																
19	107,4	110,7																
20							102,9	100,9	0,35	1,1			1	1			0,25	0,09
21	107,4	110,7																
22	107,4	110																
23	107,4	110																
24							102,2	101,6	0,35	0,5	0,75	0,7	0	0				
25	108,1	110,7																
26	106,8	110,7																
27	108,1	111,4																
28							104,2	102,9	0,35	0,8	0,65	0,7	0	0				
29	108,7	110,7																
30	109,4	111,4																
31	108,7	110,7																
32							103,5	102,9	0,35	0,45		0,6	1	0			0,2	
33		110,7																
34		110,7																
35		111,4																
36							102,9	103,5		0,35	0,78	0,45		0				
37		109,4																
38		110																
39		110																
40							103,5	104,8		0,4		0,55	1	0			0,2	
41		111,4																
42		110,7																
43		111,4																
44							104,8	108,1		0,25			1	0			0,2	
45		111,4																
46		111,4																
47		110,7																
48							103,5	110,7		0,3	0,5	0,5	0	0				
49		108,1																
50		106,8																
51		107,4																
52							102,9	108,1		0,3	0,6		0	1				
53		108,7																
54		108,7																
55		110																
56							103,5	108,1		0,09			1	1			0,15	

Average Flashover voltage with grounded plate = 102.2 Kv

Average Flashover voltage with Floating plate = 108.9 Kv

Appendix [J]: Applied PLI voltage on air medium

	Impulse charging voltage (kV)				Applied impulse voltage (KV)				Surface Potl before FOV (kV)				Flashover voltage (F		Surface pot just after FOV (kV)			
	Negative Polarity		Positive polarity		Negative Polarity		Positive polarity		Negative Polarity		Positive polarity		Grd plt FO yes = 1	Flt plt FO yes = 1	Negative Polarity		Positive polarity	
Number o	Grd plt	Flt plt	Grd plt	Flt plt	Grd plt	Flt plt	Grd plt	Flt plt	Grd plt	Flt plt	Grd plt	Flt plt	No = 0	No = 0	Grd plt	Flt plt	Grd plt	Flt plt
1	30						82,05						0					
2	30						82,05						0					
3	30						82,05						0					
4	30						82,05						0					
5	35						95,6						1					
6	35						95,1						1					
7	35						95,3						1					
8	35						95,6						1					
9	34						92,7						0					
10	34						92,7						0					
11	34						92,7						0					
12	34						92,7						0					
13	34,3						93,53						0					
14	34,3						93,53						0					
15	34,3						93,74						0					
16	34,3						93,53						0					
17	34,3						93,33						1					
18	34,3						93,53						0					
19	34,5						93,94						1					
20	34,5						93,94						1					
21	34,5						94,15						0					
22	34,5						93,74						0					
23	34,5						94,15						1					
24	34,5						94,15						0					
25	34,5						93,94						0					
26	34,5						93,94						0					
27	34,5						94,15						1					
28	34,5						93,94						1					
29	34,5						93,94						0					
30	34,5						93,94						1					
						Average Flashover voltage = 94 kV												

Appendix [K]: Measurement of surface potential distribution along a positively dc-corona charged SIR samples surface

osition (mm)	Surface potential distribution along the SIR sample surface (V)												
	5 kV test 1	5 kV test 2	5kV test 3	5kV test 4	10 kV test 1	10 kV test 2	10 kV test 3	10 kV test 4	15 kV test 1	15 kV test 2	15 kV test 3	15kV test 4	20 kV test 4
-40	-100	-87	-190	100	58	-5	-640	-670	330	-1670	560	500	550
-35	-120	-110	-190	150	97	720	-540	-950	640	480	1120	1500	840
-30	-70	-30	-260	280	180	950	-130	-920	940	300	1600	2040	1240
-25	-50	40	-250	380	250	1130	530	120	1320	630	1840	2330	1660
-20	210	80	-280	480	288	1210	1400	800	1600	870	1730	2160	1970
-15	470	150	-290	590	285	1180	1330	770	1740	1160	1580	1950	2290
-10	820	260	-310	810	135	1170	1350	1010	1950	1620	1450	1800	2480
-5	1220	400	-340	800	-60	1140	1330	1170	2170	1980	1300	1500	2380
0	1090	470	-360	720	-195	1110	1210	1250	1990	2000	1280	1430	2350
5	1090	440	-400	710	-141	1130	1300	1230	2100	2010	1360	1550	2550
10	1050	420	-480	660	273	1090	1280	1200	1840	1560	1240	1440	3080
15	770	350	-500	640	30	1030	1240	1080	1750	970	940	1070	3280
20	570	270	-430	590	-144	820	1250	900	1570	550	600	650	3190
25	420	210	-320	470	-121	570	1220	770	1440	350	337	330	2910
30	270	150	-260	650	-171	390	1130	550	1050	130	167	130	2290
35	130	100	-160	280	-20	340	1030	400	660	14	55	100	1980
40	110	80	-140	90	-122	250	880	350	470	90	60	20	1560

Measurement of surface potential decay on positively dc-corona charged SIR sample

Decay tests at center of samples						Decay tests at 10 mm from center				Decay tests at 30 mm from cent			
Time(min	Test-1	Test-2	Test-3	Aver valu	Test-1	Test-2	Test-3	Aver val 1	Test-1	Test-2	Test-3	Aver value
0	0	0	0	0	0	0	0	0	0	0	0	0
1	6196,59	6979,37	6842,04	6672,667	6823,73	5752,56	6192,02	6256,103	3523,25	3475,95	4072,57	3690,59
2	5259,7	5421,45	5421,45	5367,533	4388,43	4573,06	4388,43	4449,973	2807,62	2787,78	3240,97	2945,457
3	4940,8	4850,77	4951,48	4914,35	4927,06	4064,94	3909,3	4300,433	2438,35	2452,09	2876,28	2588,907
4	4592,9	4443,36	4557,8	4531,353	4475,4	3634,64	3486,63	3865,557	2201,84	2153,02	2574,16	2309,673
5	4296,87	4049,68	4211,43	4185,993	4063,42	3271,48	3129,58	3488,16	1924,13	1898,19	2291,87	2038,06
6	4031,37	3744,51	3916,93	3897,603	3669,74	3004,46	2883,91	3186,037	1750,18	1692,2	2082,82	1841,733
7	3793,33	3439,33	3662,11	3631,59	3350,83	2740,48	2647,4	2912,903	1567,08	1542,66	1913,45	1674,397
8	3544,62	3222,66	3404,24	3390,507	3089,9	2499,39	2418,52	2669,27	1405,33	1364,14	1699,83	1489,767
9	3384,4	2989,2	3208,92	3194,173	2836,61	2362,06	2239,99	2479,553	1318,36	1214,6	1583,86	1372,273
10	3186,04	2778,63	2999,88	2988,183	2638,24	2148,44	2070,62	2285,767	1156,62	1139,83	1458,74	1251,73
11	3007,51	2658,08	2825,93	2830,507	2453,61	1998,9	1971,44	2141,317	1095,58	1019,29	1353,45	1156,107
12	2862,55	2467,35	2648,93	2659,61	2290,34	1855,47	1834,11	1993,307	1026,92	926,21	1274,11	1075,747
13	2716,06	2305,6	2551,27	2524,31	1997,38	1747,13	1730,35	1824,953	921,63	872,8	1184,08	992,8367
14	2574,16	2194,21	2381,9	2383,423	1853,94	1638,79	1611,33	1701,353	857,54	791,93	1101,68	917,05
15	2420,04	2090,45	2290,34	2266,943	1791,38	1538,09	1501,46	1610,31	802,61	752,26	1039,12	864,6633
16	2325,44	1951,6	2192,69	2156,577	1699,83	1432,8	1416,02	1516,217	767,52	677,49	985,72	810,2433
17	2128,6	1860,05	2085,88	2024,843	1588,44	1344,3	1348,88	1427,207	724,79	668,33	933,84	775,6533
18	2024,84	1744,08	1991,27	1920,063	1527,4	1287,84	1289,37	1368,203	657,65	592,04	888,06	712,5833
19	1841,74	1676,94	1882,93	1800,537	1472,47	1237,49	1220,7	1310,22	643,92	555,42	872,8	690,7133
20	1750,18	1582,34	1811,22	1714,58	1374,82	1177,98	1106,26	1219,687	598,14	523,38	793,46	638,3267

Pote distr on SIR sample at time (t=1 mi

Position		T=1 min	
3	3523,25	3475,95	4072,57
1	6823,73	5752,56	6192,02
0	6196,59	6979,37	6842,04
-1	6823,73	5752,56	6192,02
-3	3523,25	3475,95	4072,57

Pote distr on SIR sample at time (t=3 min)

Position		T=3 min	
3	2438,35	2452,09	2876,28
1	4927,06	4064,94	3909,3
0	4940,8	4850,77	4951,48
-1	4927,06	4064,94	3909,3
-3	2438,35	2452,09	2876,28

Pote distr on SIR sample at time (t=2 mi

Position		T=2 min	
3	2807,62	2787,78	3240,97
1	4388,43	4573,06	4388,43
0	5259,7	5421,45	5421,45
-1	4388,43	4573,06	4388,43
-3	2807,62	2787,78	3240,97

Pote distr on SIR sample at time (t=5 min)

Position		T=5 min	
3	1924,13	1898,19	2291,87
1	4063,42	3271,48	3129,58
0	4296,87	4049,68	4211,43
-1	4063,42	3271,48	3129,58
-3	1924,13	1898,19	2291,87

Pote distr on SIR sample for time (t=1,2,3 & 5 min)

Position	T=1min	T=2 min	T=3 min	T=5 min
3	3690,59	2945,46	2588,91	2038,063
1	6256,1	4449,97	4300,43	3488,16
0	6672,67	5367,53	4914,35	4185,99
-1	6256,1	4449,97	4300,43	3488,16
-3	3690,59	2945,46	2588,91	2038,063

Appendix [L]: Measurement of potential decay on a negatively dc-corona charged SIR sample

Measurements of the surface potential distribution on a negatively dc-corona charged SIR sample

e Position	Measured spatial and temporal potential distribution on a negatively dc-corona charged SIR samples (V)																	
	5 kv trail 1	5 kv trail 2	5 kv trail 3	5 kv trail 4	V Average val	10 kv trial 1	10 kv trial 2	10 kv trial 3	kV Average va	15 kv trail 1	15 kv trail 2	15 kv trail 3	15 kv trail 4	15 kv trail 5	alue for -15	20 kv trail 1	20 kv trail 2	Average v
-40	-0,68	-0,29	0,25	0,06	-0,165	-0,32	-0,45	-0,41	-0,39333333	-0,62	-1,73	-0,05	-0,84	-0,05	-0,658	-1,43	-0,59	-1,01
-35	-0,77	-0,37	0,32	0,05	-0,1925	-0,41	-0,63	-0,51	-0,51666667	-1	-2,27	-0,41	-1,31	-0,48	-1,094	-1,94	-0,44	-1,19
-30	-1	-0,5	0,36	0,017	-0,28075	-0,62	-0,83	-0,7	-0,71666667	-1,23	-2,38	-0,34	-1,43	-0,82	-1,24	-2,37	0,05	-1,16
-25	-1,22	-0,65	0,34	-0,034	-0,391	-0,89	-1,07	-0,93	-0,96333333	-1,33	-2,42	-0,92	-1,41	-1,17	-1,45	-2,66	-1,58	-2,12
-20	-1,43	-0,81	0,28	-0,092	-0,513	-1,16	-1,26	-1,14	-1,18666667	-1,6	-2,74	-2,01	-1,77	-1,63	-1,95	-3,12	-2,39	-2,755
-15	-1,64	-0,96	0,16	-0,15	-0,6475	-1,39	-1,64	-1,64	-1,55666667	-1,88	-3,01	-2,94	-2,06	-2,17	-2,412	-3,4	-2,85	-3,125
-10	-1,83	-1,15	-0,05	-0,23	-0,815	-1,62	-2,01	-1,73	-1,78666667	-2,08	-3,28	-3,38	-2,14	-2,58	-2,692	-3,4	-3,07	-3,235
-5	-1,9	-1,33	-0,33	-0,35	-0,9775	-1,81	-2,36	-1,84	-2,00333333	-2,2	-3,4	-3,38	-2,09	-2,89	-2,792	-3,4	-3,13	-3,265
0	-1,83	-1,38	-0,53	-0,44	-1,045	-1,84	-2,55	-1,85	-2,08	-2,15	-3,4	-3,38	-2,08	-2,88	-2,778	-3,4	-3,09	-3,245
5	-1,74	-1,37	-0,59	-0,4	-1,025	-1,7	-2,34	-1,72	-1,92	-2,13	-3,36	-3,38	-2,08	-2,84	-2,758	-3,4	-2,89	-3,145
10	-1,67	-1,23	-0,53	-0,25	-0,92	-1,41	-1,94	-1,44	-1,59666667	-2,04	-2,95	-2,74	-1,82	-2,51	-2,412	-3,4	-2,48	-2,94
15	-1,47	-1	-0,39	-0,11	-0,7425	-1,11	-1,54	-1,11	-1,25333333	-1,83	-2,55	-2,07	-1,35	-1,98	-1,956	-3,11	-2,28	-2,695
20	-1,21	-0,89	-0,27	-0,026	-0,599	-0,91	-1,26	-0,86	-1,01	-1,59	-2,22	-1,6	-0,93	-1,5	-1,568	-2,67	-2,11	-2,39
25	-0,91	-0,81	-0,14	0,04	-0,455	-0,74	-0,95	-0,61	-0,76666667	-1,32	-1,91	-1,22	-0,62	-1,19	-1,252	-2,27	-1,94	-2,105
30	-0,66	-0,7	-0,01	0,096	-0,3185	-0,61	-0,67	-0,38	-0,55333333	-1,04	-1,62	-0,94	-0,4	-1	-1	-1,86	-1,67	-1,765
35	-0,47	-0,56	0,09	0,11	-0,2075	-0,51	-0,46	-0,24	-0,40333333	-0,8	-1,34	-0,79	-0,34	-0,84	-0,822	-1,48	-1,33	-1,405
40	-0,35	-0,43	0,14	0,077	-0,14075	-0,43	-0,36	-0,15	-0,31333333	-0,61	-1,13	-0,62	-0,38	-0,68	-0,684	-1,17	-0,93	-1,05

Measurement of surface potential decay on a negatively dc-corona charged SIR samples

Time (min)	#VALUE!	V decay te	V decay te	charging k	kV decy te	V decay te
0	6	0	0	-1,2	0	0
1	66	-2060	-2360	-1,78	-1620,5	-1518,3
2	126	-2020	-2200	-1,35	-1623,5	-1641,9
3	186	-1880	-2040	-1,06	-1489,2	-1539,6
4	246	-1740	-1900	-0,84	-1287,8	-1379,4
5	306	-1610	-1800	-0,69	-1106,2	-1210
6	366	-1490	-1650	-0,57	-952,1	-1080,3
7	426	-1380	-1540	-0,48	-850	-958,3
8	486	-1290	-1440	-0,4	-718,7	-849,9
9	546	-1200	-1360	-0,34	-639,3	-761,4
10	606	-1120	-1280	-0,29	-518,8	-679
11	666	-1050	-1200	-0,26	-431,8	-589
12	726	-990	-1140	-0,22	-373,8	-509,6
13	786	-930	-1080	-0,2	-326,5	-491,3
14	846	-870	-1020	-0,17	-273,1	-444
15	906	-830	-960	-0,15	-242,6	-398,3
16	966	-780	-910	-0,13	-190,7	-328
17	1026	-740	-860	-0,12	-169,4	-282,3
18	1086	-700	-810	-0,11	-167,9	-231,9
19	1146	-670	-770	-0,1	-123,6	-213,6
20	1206	-630	-730	-0,09	-94,6	-195,3

Appendix [M]: Measurement of surface potential decay and distribution on positively dc-corona charged RTV-SIR samples

Measurement of surface potential distribution on a positively dc-corona charged RTV-SIR sample at four different times

Time = 1 min

Position (	M1	M2	M3	M4	Average
-30	5770	5630	5220	5850	5617,5
-10	8070	7320	8710	8430	8132,5
0	9070	8120	8140	7500	8207,5
10	8070	7320	8710	8430	8132,5
30	5770	5630	5220	5850	5617,5

Time = 3 min

Position (	M1	M2	M3	M4	Average
-30	2360	2170	2020	1920	2117,5
-10	2000	1880	1790	1770	1860
0	1620	1680	1720	1870	1722,5
10	2000	1880	1790	1770	1860
30	2360	2170	2020	1920	2117,5

Time = 2 min

Position (	M1	M2	M3	M4	Average
-30	3140	2890	2730	2570	2832,5
-10	2930	2750	2610	2570	2715
0	2540	2640	2670	2740	2647,5
10	2930	2750	2610	2570	2715
30	3140	2890	2730	2570	2832,5

Time = 5 min

Position (	M1	M2	M3	M4	Average
-30	1490	1370	1250	1240	1337,5
-10	1190	1110	1060	1030	1097,5
0	1210	1240	1410	1390	1312,5
10	1190	1110	1060	1030	1097,5
30	1490	1370	1250	1240	1337,5

Measurement of surface potential decay on positively dc-corona charged RTV-SIR samples at three different positions

Measurement of surface decay test at center on positively dc-corona charged RTV-SIR samples

Time (min)	y test 1 at ce	ay test 2 at cen	ay test 3 at cen	ay test 4 at cen	ay test 5 at ce	cay test 6 at cen	ay test at cen
1	8120	8140	7500	7420	8680	8010	7978,33333
2	2640	2670	2740	2650	3060	2650	2735
3	1680	1720	1870	1810	2100	1730	1818,33333
4	1210	1240	1410	1390	1600	1280	1355
5	920	980	1110	1100	1270	1010	1065
6	750	790	900	890	1030	790	858,333333
7	620	640	750	750	850	670	713,333333
8	520	550	640	630	720	560	603,333333
9	430	490	550	550	600	510	521,666667
10	380	420	490	470	520	430	451,666667
11	330	360	410	400	450	370	386,666667
12	250	330	360	350	390	320	333,333333
13	220	280	310	300	340	300	291,666667
14	220	260	280	270	310	250	265
15	190	230	240	230	270	260	236,666667
16	170	200	230	210	230	220	210
17	150	170	200	190	220	220	191,666667
18	130	170	170	150	190	180	165
19	130	160	160	140	160	170	153,333333
20	130	130	140	140	150	160	141,666667

Decay measurements at 10 mm from center

Time min	decay test 1 a	decay test 2 at	decay test 3 at	decay test 4 at	r decay at 10 mm
1	8070	7320	8710	8430	8132,5
2	2930	2750	2610	2570	2715
3	2000	1880	1790	1770	1860
4	1510	1400	1340	1320	1392,5
5	1190	1110	1060	1030	1097,5
6	950	870	850	840	877,5
7	790	700	690	690	717,5
8	660	610	590	580	610
9	540	520	490	480	507,5
10	460	420	420	400	425
11	400	370	360	350	370
12	350	320	310	290	317,5
13	310	270	270	250	275
14	260	240	240	220	240
15	230	230	220	200	220
16	200	190	190	200	195
17	170	160	160	140	157,5
18	160	150	150	140	150
19	140	130	120	130	130
20	130	110	110	130	120

Decay measurements at 30 mm from center					
Time (min)	y test 1 at 30	cay test 2 at 30 r	cay test 3 at 30 k	Kv D-test 4 at 3	d-test at 30 n
1	5770	5630	5220	5850	5617,5
2	3140	2890	2730	2570	2832,5
3	2360	2170	2020	1920	2117,5
4	1870	1690	1580	1520	1665
5	1490	1370	1250	1240	1337,5
6	1230	1100	1040	1000	1092,5
7	1030	890	830	800	887,5
8	860	760	710	690	755
9	750	650	590	570	640
10	610	560	520	480	542,5
11	540	470	430	420	465
12	450	400	370	360	395
13	370	360	320	310	340
14	360	340	300	270	317,5
15	310	290	260	250	277,5
16	280	250	200	220	237,5
17	230	250	190	190	215
18	210	220	190	170	197,5
19	183	170	160	140	163,25
20	180	190	140	150	165

Appendix [N]: Measurement of surface potential distribution and decay on negatively dc-corona charged RTV-SIR samples

Measurement of surface potential distribution on a negatively dc-corona charged RTV-SIR sample at four different times

Time = 1 min

Position	M1	M2	M3	Average
-30	-3910	-3940	-2800	-3550
-10	-4250	-4060	-5400	-4570
0	-5016	-5057	-4512	-4861,67
10	-4250	-4060	-5400	-4570
30	-3910	-3940	-2800	-3550

Time = 3 min

Position	M1	M2	M3	Average
-30	-1390	-1420	-1130	-1313,33
-10	-1310	-1210	-1400	-1306,67
0	-1210	-1030	-906	-1048,67
10	-1310	-1210	-1400	-1306,67
30	-1390	-1420	-1130	-1313,33

Time = 2 min

Position	M1	M2	M3	Average
-30	-1870	-1940	-1510	-1773,33
-10	-1810	-1710	-2040	-1853,33
0	-1740	-1460	-1280	-1493,33
10	-1810	-1710	-2040	-1853,33
30	-1870	-1940	-1510	-1773,33

Time = 5 min

Position	M1	M2	M3	Average
-30	-910	-900	-650	-820
-10	-840	-740	-860	-813,333
0	-726	-635	-565	-642
10	-840	-740	-860	-813,333
30	-910	-900	-650	-820

Measurement of surface potential decay on a negatively dc-corona charged RTV-SIR samples at three different positions

Decay measuerments at center

time (min	Kv decay tes	5Kv decay test	5 Kv decay test	15 Kv decay test 4	Kv decay tes	5 Kv decay test	eg decay meas
1	-4950	-3590	-5016	-5057	-4512	-4460	-4597,5
2	-1740	-1460	-1807	-1936	-1890	-1660	-1748,8333
3	-1210	-1030	-1260	-1321	-1300	-1130	-1208,5
4	-928	-780	-961	-1001	-989	-851	-918,33333
5	-726	-635	-752	-807	-801	-680	-733,5
6	-623	-542	-636	-685	-661	-565	-618,66667
7	-536	-461	-546	-591	-566	-470	-528,33333
8	-455	-409	-465	-500	-490	-403	-453,66667
9	-397	-354	-412	-455	-435	-368	-403,5
10	-339	-314	-369	-398	-389	-318	-354,5
11	-304	-285	-332	-365	-342	-281	-318,16667
12	-308	-246	-311	-320	-302	-247	-289
13	-267	-233	-276	-290	-290	-233	-264,83333
14	-241	-220	-261	-269	-260	-214	-244,16667
15	-218	-206	-235	-230	-230	-191	-218,33333
16	-208	-186	-201	-204	-204	-179	-197
17	-180	-159	-185	-191	-197	-160	-178,66667
18	-169	-153	-177	-185	-179	-140	-167,16667
19	-156	-136	-148	-169	-165	-136	-151,66667
20	-157	-134	-150	-163	-162	-125	-148,5

Decay measurements at 10 mm from center

Time (min	Kv decay tes	5Kv decay test	5 Kv decay test	Averga
1	-4250	-4060	-5400	-4570
2	-1810	-1710	-2040	-1853,333333
3	-1310	-1210	-1400	-1306,666667
4	-1020	-920	-1100	-1013,333333
5	-840	-740	-860	-813,3333333
6	-690	-600	-710	-666,6666667
7	-600	-510	-610	-573,3333333
8	-530	-440	-540	-503,3333333
9	-470	-320	-470	-420
10	-420	-280	-410	-370
11	-370	-252	-370	-330,6666667
12	-342	-250	-340	-310,6666667
13	-310	-210	-302	-274
14	-290	-210	-290	-263,3333333
15	-250	-180	-260	-230
16	-230	-170	-240	-213,3333333
17	-220	-150	-230	-200
18	-220	-130	-214	-188
19	-180	-140	-190	-170
20	-183	-130	-182	-165

Decay measurements at 30 mm from center

Time (min)	ecay test 1at	ecay test 2 at	ecay test 3 at 30 mm	
1	-3910	-3940	-2800	-3550
2	-1870	-1940	-1440	-1750
3	-1390	-1420	-1040	-1283,333333
4	-1110	-1110	-810	-1010
5	-910	-900	-650	-820
6	-770	-760	-560	-696,6666667
7	-680	-650	-480	-603,3333333
8	-590	-570	-420	-526,6666667
9	-523	-510	-380	-471
10	-480	-451	-280	-403,6666667
11	-430	-400	-280	-370
12	-400	-360	-250	-336,6666667
13	-340	-330	-234	-301,3333333
14	-320	-300	-220	-280
15	-300	-280	-190	-256,6666667
16	-290	-270	-170	-243,3333333
17	-240	-240	-170	-216,6666667
18	-230	-220	-160	-203,3333333
19	-220	-220	-170	-203,3333333
20	-210	-180	-160	-183,3333333